Biomaterials Science

ROYAL SOCIETY OF CHEMISTRY

PAPER

View Article Online
View Journal | View Issue

Cite this: *Biomater. Sci.*, 2024, **12**, 4770

Biological effects of a zinc-substituted borosilicate bioactive glass on human bone marrow derived stromal cells *in vitro* and in a critical-size femoral defect model in rats *in vivo*

M. Saur, †[a] E. Kunisch,†[a] L. A. Fiehn, [a] M. Arango-Ospina, [b] C. Merle,[a,c] S. Hagmann,[a] A. Moghaddam,[d] A. Stiller,[e] L. Hupa,[e] T. Renkawitz,[a] H. Kaňková,[f] D. Galusková, [f] A. R. Boccaccini *[b] and F. Westhauser *[a]

The borosilicate 0106-B1-bioactive glass (BG) composition (in wt%: 37.5 SiO_2, 22.6 CaO, 5.9 Na_2O, 4.0P_2O_5, 12.0 K_2O, 5.5 MgO, 12.5 B_2O_3) has shown favorable processing characteristics and bone regeneration ability. This study investigated the addition of zinc (Zn) to 0106-B1-BG as an approach to improve this BG's biological properties. Different proportions of ZnO were substituted for CaO in 0106-B1-BG, resulting in three new BG-compositions: 1-Zn-BG, 2-Zn-BG, 3-Zn-BG (in wt%: 37.5 SiO_2, 21.6/20.1/17.6 CaO, 4.0 P_2O_5, 5.9 Na_2O, 12.0 K_2O, 5.5 MgO, 12.5 B_2O_3 and 1.0/2.5/5.0 ZnO). Effects of the BG compositions on cytocompatibility, osteogenic differentiation, extracellular matrix deposition, and angiogenic response of human bone marrow-derived mesenchymal stromal cells (BMSCs) were evaluated *in vitro*. Angiogenic effects were assessed using a tube formation assay containing human umbilical vein endothelial cells. The *in vivo* osteogenic and angiogenic potentials of 3-Zn-BG were investigated in comparison to the Zn-free 0106-B1-BG in a rodent critical-size femoral defect model. The osteogenic differentiation of BMSCs improved in the presence of Zn. 3-Zn-BG showed enhanced angiogenic potential, as confirmed by the tube formation assay. While Zn-doped BGs showed clearly superior biological properties *in vitro*, 3-Zn-BG and 0106-B1-BG equally promoted the formation of new bone *in vivo*; however, 3-Zn-BG reduced osteoclastic cells and vascular structures *in vivo*. The acquired data suggests that the differences regarding the *in vivo* and *in vitro* results may be due to modulation of inflammatory responses by Zn, as described in the literature. The inflammatory effect should be investigated further to promote clinical applications of Zn-doped BGs.

Received 17th April 2024,
Accepted 4th August 2024

DOI: 10.1039/d4bm00529e

rsc.li/biomaterials-science

1 Introduction

The composition of 45S5-BG (in wt%: 45.0 SiO_2, 24.5 Na_2O, 24.5 CaO, 6.0 P_2O_5), introduced in the 1960s by Larry Hench,[1] is considered as the benchmark amongst BGs and has established itself in both experimental and clinical bone tissue repair. Despite its excellent biological qualities, 45S5-BG has some limits: an initial release of sodium ions increases pH, which might harm cells in standard cell culture settings.[2,3] Furthermore, sintering three-dimensional scaffolds is difficult because 45S5-BG tends to crystallize at high temperatures.[4,5] To overcome these limitations, various other BG compositions with a low crystallization tendency have been developed over the years, enabling the production of porous three-dimensional non-crystalline scaffolds.[4,6,7] One example is BG 1393 (in wt%: 53.0 SiO_2, 20.0 CaO, 6.0 Na_2O, 4.0 P_2O_5, 12.0 K_2O, 5.0 MgO) and the related BG composition 0106 (in wt% 50.0 SiO_2, 22.6 CaO, 5.9 Na_2O, 4.0 P_2O_5, 12.0 K_2O, 5.3 MgO, 0.2 B_2O_3).[8] Considering the positive biological effect of boron, a new BG composition, termed 0106-B1, was designed and reported for the first time in 2016, in which B_2O_3 was substituted partially for SiO_2. 0106-B1-BG (in wt%: 37.5 SiO_2, 22.6 CaO, 5.9 Na_2O, 4.0 P_2O_5, 12.0 K_2O, 5.5 MgO, 12.5 B_2O_3) was reported to exhibit good bioactivity and pro-angiogenic properties *in vitro*.[8,9]

[a]*Department of Orthopaedics, Heidelberg University Hospital, Schlierbacher Landstraße 200a, 69118 Heidelberg, Germany. E-mail: Fabian.Westhauser@med.uni-heidelberg.de*
[b]*Institute of Biomaterials, University of Erlangen-Nuremberg, Cauerstr. 6, 91058 Erlangen, Germany. E-mail: aldo.boccaccini@fau.de*
[c]*Joint Replacement Centre, Orthopaedic Surgery Paulinenhilfe, Diakonie-Klinikum Stuttgart, Rosenbergstraße 38, 70176 Stuttgart, Germany*
[d]*Privatärztliches Zentrum Aschaffenburg, Frohsinnstraße 12, 63739 Aschaffenburg, Germany*
[e]*Johan Gadolin Process Chemistry Centre, Åbo Akademi University, Henrikinkatu 2, 20500 Turku, Finland*
[f]*Centre for Functional and Surface Functionalized Glass, Alexander Dubček University of Trenčín, Študentská 2, 911 50 Trenčín, Slovakia*
†These authors contributed equally to this work.

Further, 0106-B1-BG not only shows improved sintering ability,[8] but the addition of boron (B) also allows for widening the biological properties: B is known for its pro-angiogenic effects *in vitro* and stimulation of bone healing *in vivo*.[10,11]

Recently, a comparative study conducted by our group suggested that 1393-BG and 0106-B1-BG had improved proliferation and viability of human bone marrow-derived mesenchymal stromal cells (BMSCs) compared to 45S5-BG.[12] Compared to 45S5-BG and 0106-B1-BG, 1393-BG demonstrated superior osteogenic properties *in vitro*. However, *in vivo* – in a segmental bone defect of critical size in a rodent model – 45S5-BG and 0106-B1-BG showed increased new bone formation compared to 1393-BG. In addition, 0106-B1-BG significantly improved angiogenesis *in vitro* and *in vivo* compared to 1393-BG. The results confirmed that targeted modification of BG compositions directly influences the BGs' biological effects – in this case, the addition of pro-angiogenic B improved the osteogenic and angiogenic properties.

Aiming at further improving the biological properties of the 0106-B1-BG composition, different ions can be substituted. A CuO-containing 0106-B1-BG was shown to have improved osteogenic and angiogenic properties *in vitro* compared to the undoped 0106-B1-BG; *in vivo* there were no significant differences in the performance of the glasses.[13] In order to investigate the effect of other promising ions, zinc (Zn) was incorporated in the 0106-B1-BG, since Zn has been shown to not only induce anti-inflammatory effects but also stimulate bone formation by regulation of osteoblastic differentiation markers like alkaline phosphatase (ALP), collagen I, osteopontin (OPN) and osteocalcin (OCN).[14,15] As part of either mesoporous bioactive glass nanoparticles (MBGNs) or in the form of ZnO containing 1393-BG, Zn improved the osteogenic properties of the parent materials.[16,17] Therefore, in this study, Zn was added to the 0106-B1-BG composition by substituting ZnO for CaO, resulting in three new BG compositions (1-Zn, 2-Zn, and 3-Zn) containing an increasing portion of Zn (1 wt%, 2.5 wt%, 5 wt% ZnO). In the *in vitro* part of this study, the dose-dependent properties of Zn were assessed by cultivating BMSCs in direct contact with the BGs, focusing on proliferation, viability, osteogenic differentiation, and angiogenic growth factor expression. To further characterize the angiogenic potential of Zn-containing 0106-B1-BG variants, a tube formation assay was performed, using human umbilical vein endothelial cells (HUVECs). In the *in vivo* part of this study, 3-Zn-BG and Zn-free 0106-B1-BG 3D scaffolds were implanted into critical-size bone defects in rodent femurs. The focus of interest hereby was bone regeneration, vascularisation, and activation of osteoclasts, causal for degradation of the scaffolds during the regeneration process. The main goal was thus to provide data to confirm whether adding Zn to 0106-B1-BG will further improve its biological properties with a focus on bone regeneration.

2 Materials and methods

2.1 Bioactive glasses

The nominal compositions of the BGs used are listed below (Table 1). 1-Zn, 2-Zn and 3-Zn-BGs contain increasing Zn concentrations.

2.2 Production and characterization of BGs and scaffolds

The production of BGs was conducted using the melt-quench technique, as previously described for the 0106-B1-BG.[8] The same analytical grade reagents as 0106-B1-BG were used to produce the Zn-containing compositions, and Zn was added as ZnO (Sigma-Aldrich, Germany). BGs were melted in Pt crucibles at 1360 °C for 1.5 hours, followed by annealing for 1 hour at 520 °C. After cooling, the samples were processed to fine particles of less than 38 μm in size utilizing a Jaw Crusher BB 51, a planetary ball mill PM100 and a 38 μm sieve from Retsch, Germany. The particles used for the *in vitro* studies were thermally treated using the same parameters (described below) applied for sintering of the 3D porous scaffolds used for the *in vivo* studies. This process was necessary to ensure similar thermal history and thus the same BG structure of the particles and the 3D scaffolds. After the thermal treatment, the particles were sieved to below 38 microns and incubated in DMEM for up to 21 days for ion release studies. The BG particles were preconditioned in a concentration of 1 mg ml^{-1} in an orbital shaker at 300 rpm and 37 °C for 24 hours; then, the supernatant was collected after centrifugation at 4000 rpm for 10 minutes. The particles were resuspended in fresh DMEM and incubated at 37 °C and 5% CO_2. After 1, 3, 7, 10, 14, 17 and 21 days, the supernatant was collected, and fresh medium was added. The samples were then kept for analysis after being stabilized with nitric acid (pH < 2). The concentration of silicon, boron, zinc and phosphorous ions released from the BG particles was quantified using an inductively coupled plasma-optical emission spectrometer (ICP-OES, Agilent 5100 SVDV, Agilent Technologies, Inc., USA). Moreover, sintered and unsintered glass particles were evaluated with an X-ray diffractometer (Miniflex 600 HR, Rigaku, Neu-Isenburg, Germany) over the 2θ

Table 1 Nominal compositions of the used bioactive glasses

Composition [wt%]	SiO_2	CaO	Na_2O	P_2O_5	K_2O	MgO	B_2O_3	ZnO
0106-B1-BG	37.5	22.6	5.9	4.0	12.0	5.5	12.5	
1-Zn-BG	37.5	21.6	5.9	4.0	12.0	5.5	12.5	1.0
2-Zn-BG	37.5	20.1	5.9	4.0	12.0	5.5	12.5	2.5
3-Zn-BG	37.5	17.6	5.9	4.0	12.0	5.5	12.5	5.0

The components of the BGs are given in % by weight. For the 1-Zn, 2-Zn and 3-Zn-BGs, ZnO is used as a substitute for CaO.

range from 10° to 60° and a step size of 0.02°. Particle size distribution of sintered BG particles was determined *via* laser diffraction analysis using a Mastersizer 3000 (Malvern Panalytical, UK) under wet conditions in deionized water.

The foam replica technique[5] was used to produce 3D scaffolds from the glass powders. Cylindrical polyurethane foams of 45 ppi (Pahlke Schaumstoffe, St Katharinen, Germany) were used as sacrificial templates to obtain highly porous structures. As previously described for the production of borosilicate 0106-B1-BG scaffolds,[8,12] ethanol was used as a solvent to generate a slurry with 50 wt/vol% of BG and 3.5 wt/vol% of ethylcellulose which acted as a binder. Dip-coating of the foams was then performed, followed by drying and sintering in which the green bodies were initially exposed to a temperature of 400 °C for 1 hour to remove the polymer foam and then heated to the adequate densification temperature, 600 °C for 1-Zn-BG and 585 °C for 2- and 3-Zn-BG, with a dwell time of 3 hours and a heating rate of 2 °C min^{-1} for all samples. To achieve dense scaffolds, the 1-Zn-BG composition required a different sintering temperature because using the same settings as other BG compositions resulted in partial fusion of BG particles producing rough struts where individual particles could be seen, leading to brittle scaffolds. Furthermore, a higher crystallization temperature was found for 1-Zn-BGs in comparison to the other BG formulations through thermal analysis by differential scanning calorimetry. This observation allowed for an increase in the sintering temperature while maintaining the amorphous structure. Scanning electron microscopy (SEM, Auriga, Carl-Zeiss, Jena, Germany) at a voltage of 1.5 kV was used to examine the morphology of the scaffolds. The compressive strength of sintered BG scaffolds was measured using the universal testing machine Instron 5967 (Instron GmbH Darmstadt, Germany) with a 100 N load cell and a crosshead speed of 5 mm min^{-1}.

2.3 *In vitro* experiments

2.3.1 Study ethics and cell origin. BMSCs were harvested from 5 male (mean age 59 ± 15 years) and 5 female patients (mean age 56 ± 11 years) undergoing hip arthroplasty and pooled in passage 1 as previously described.[18] All experiments were performed in accordance with the declaration of Helsinki in its present form, and experiments were approved by the ethics committee at the Medical Faculty of the University of Heidelberg (S-340/2018). Written consents were obtained from human participants of this study.

2.3.2 Cell isolation and cultivation. The patient material was intra-operatively collected, and BMSCs were isolated as described in ref. 18. After a washing step with Dulbecco's phosphate buffered saline (DPBS without Mg^{2+} and Ca^{2+}, Thermo Fisher Scientific, Dreieich, Germany, if not mentioned otherwise in the following DPBS always refers to this), bone marrow was applied to density gradient centrifugation using Ficoll-Paque Plus (GE Healthcare Bio-Sciences, Uppsala, Sweden). Expansion medium containing Dulbecco's modified Eagle's medium (DMEM; Thermo Fisher Scientific) supplemented with 12.5% fetal calf serum (FCS), 2 mM L-glutamine, 1% nonessential amino acids (NEAA), 50 μM β-mercaptoethanol (all Thermo Fisher Scientific), 100 μg ml^{-1} penicillin/streptomycin (P/S; Biochrom, Berlin, Germany), and 4 ng ml^{-1} human fibroblast growth factor 2 (FGF2; Active Bioscience, Hamburg, Germany) was used for cell cultivation. Medium change was performed after 24 h to remove nonadherent cells. At 80% confluency, passaging and pooling of BMSCs took place in passage 1. The BMSCs were stored in liquid nitrogen until further use. Cells were characterized as BMSCs as described.[12]

2.3.3 Overview of general experimental design *in vitro*. For cultivation, a cell culture medium (CCM; DMEM supplemented with 10% FCS and 100 μg ml^{-1} P/S) containing 1 mg ml^{-1} of BG particles was used. BG particles were preconditioned for 24 h in DMEM and 100 μg ml^{-1} P/S.[2] As a control group, BMSCs were cultured in BG-free CCM. Seeding of cells took place in passage 4 with a density of 2×10^4 cells per cm^2. Every group consisted of six biological replicates. The medium was changed twice weekly. On day 7 (D7) and day 21 (D21), cell number, cell viability, gene expression levels as well as osteogenic and angiogenic factor secretion were assessed.

2.3.4 Cell quantification assay. Quantification of cell number was carried out according to a previously described procedure[12] by nuclear staining with 4′,6-diamidino-2-phenylindole (DAPI; Thermo Fisher Scientific). In short, washing of cells with DPBS was followed by fixation with 70% ethanol (SERVA, Heidelberg, Germany). After air drying, incubation in staining solution for 5 min took place and the elution of bound DAPI occurred in order to measure fluorescence intensity (FI) at 355/460 nm (ex/em) using a fluorescence microplate reader (Wallac 1420 Victor 2, PerkinElmer, Waltham, USA).

2.3.5 Cell growth patterns and qualitative evaluation of cell viability. For the visualisation of cell morphology and cell growth patterns, a fluorescence microscopy-based live/dead assay was used, as described previously.[19] After a washing step, BMSCs were incubated with 6 μM fluorescein diacetate (FDA; Sigma-Aldrich, Steinheim, Germany) in DPBS for 2 min at 37 °C following removal of the staining solution. After washing and adding propidium iodide (PI; 0.2 μg ml^{-1} DPBS), fluorescence was captured using an Olympus IX-81 inverted fluorescence microscope (Olympus, Hamburg, Germany). ImageJ software (U.S. National Institutes of Health, Bethesda, MD, USA) was used to merge green and red channels.

2.3.6 Combined ALP activity and cell viability assay. A combined fluorescence-based assay was used to quantify ALP activity and FDA conversion. The addition of 2 μg ml^{-1} FDA for 5 min at 37 °C was followed by incubation in 0.5% Triton-X-100 (Sigma-Aldrich) for 5 min at 37 °C, 100 μM 4-methylumbelliferone-phosphate (4-MUP, Thermo Fisher Scientific) was added for 15 min. FI was measured at 485/535 nm (ex/em) for FDA and 360/440 nm (ex/em) for 4-MUP. As standard for ALP activity, shrimp alkaline phosphate (Thermo Fisher Scientific) was used (range 0.15 to 10 mU/50 μl).

2.3.7 mRNA expression level *in vitro* of osteogenic and angiogenic genes. For determining gene expression levels of osteogenic and angiogenic markers, qualitative polymerase chain reaction (qPCR) was used. Supernatants were collected and stored at −20 °C to be used for protein analysis. PureLink

RNA mini kit (Thermo Fisher Scientific) was applied following the manufacturer's instructions to isolate total RNA, to synthesize complementary DNA (cDNA), the high-capacity RNA-to-cDNA kit (Thermo Fisher Scientific) was applied. PowerUp SYBR green master mix (Thermo Fisher Scientific) and the listed primers (Eurofins Genomics, Ebersberg, Germany) in Table 2 were used to perform qPCR (LineGene 9600; Hangzhou Bioer Technology, Hangzhou, China). With the ΔΔCt method, relative gene expression was calculated and related to reference gene; then normalized to control group.

2.3.8 Evaluation of protein secretion of osteogenic and angiogenic proteins by ELISA. OPN, VEGF, PlGF and EDN1 secretions were quantified using ELISA assays (all R&D Systems, Wiesbaden, Germany), following the manufacturer's instructions. The SUNRISE-BASIC TECAN reader (Tecan Austria, Grödig, Austria) was used to quantify the color reaction at a wavelength of 450 nm with wavelength correction at 540 nm.

2.3.9 Tube network formation assay using HUVECs. HUVECs (Thermo Fisher Scientific) were cultivated in 200PRF (M200) medium containing low serum growth supplements (LSGS). To obtain BMSCs/BG-conditioned media, BMSCs were cultivated with the BG particles at 1 mg ml^{-1} in DMEM/10% FCS. 24 h after seeding, the medium was exchanged to M200 containing 2% FCS and incubated for three days. Supernatants of the BMSCs/BG co-cultures were collected and centrifuged; supernatants were stored at −80 °C until further use. In preparation for the tube formation assay, coating of 96-well plates, each well with 30 µl ice-cold Geltrex reduced growth factor basement membrane matrix (Thermo Fisher Scientific) was performed and left on ice for 5 min, further 10 min incubation at room temperature and 30 min at 37 °C. 2×10^4 HUVECs (passage 4) per well were seeded on the solidified gel and cultured overnight. M200 with or without LSGS was used as positive and negative controls. After 13 h, staining of the cells with calcein-AM (0.5 µg ml^{-1}; Biotium, Fremont, CA, USA) for 15 min was performed. HUVECs tube network formation was documented with phase contrast microscopy, and the tube network was assessed using a fluorescence microscope (Keyence BZ-X810, Neu-Isenburg, Germany). Quantification of the number of junctions and the total master segment length was performed with the Angiogenesis analyzer tool using the ImageJ program.[20]

Table 2 Primer for qPCR. Alkaline phosphatase (ALP), osteopontin (OPN), osteocalcin (OCN) and type I collagen alpha 1 (COL1A1) as osteogenic markers were used. For angiogenic gene expression, vascular endothelial growth factor (VEGF), placental growth factor (PlGF) and endothelin-1 (EDN1). Tyrosine 3-monooxygenase/tryptophan 5-monooxygenase activation protein zeta (YWHAZ) served as a reference gene

Gene	Primer sequence (forward; FW/reverse; REV)	Product length (bp)	Accession number
ALP	FW: gca cct gcc tta cta act c REV: aga cac cca tcc cat ctc	161	NM_000478
COL1A1	FW: tgg agc aag agg cga gag REV: cac cag cat cac cct tag c	121	NM_000088
EDN1	FW: aag aca aac cag gtc gga ga REV: tgg agg cta tgg ctt cag ac	153	NM_001168319
OCN	FW: acc gag aca cca tga gag cc REV: gct tgg aca caa agg ctg cac	138	NM_199173.6
OPN	FW: gct aaa ccc tga ccc atc tc REV: ata act gtc ctt ccc acg g	546	NM_001040058.2
PlGF	FW: tca gag gtg gaa gtg gta ccc t REV: acg gat ctt tag gag ctg cat	224	NM_002632
VEGF	FW: ggg cag aat cat cac gaa g REV: atc tgc atg gtg atg ttg ga	217	NM_001025366
YWHAZ	FW: tgc ttg cat ccc aca gac ta REV: agg cag aca atg aca gac ca	126	NM_003406.4

2.4 *In vivo* experiments

2.4.1 Overview of general experimental design *in vivo*. The animals received a critical-size defect on the left femur. The study consisted of four experimental groups including seven animals each: one group of control animals with an empty defect, the defect of one group was filled 1393-BG, one with 0106-B1-BG, and the last group with 3-Zn-BG, presenting as the most promising Zn-containing BG composition in the *in vitro* part of the study according to the 3-R (replace, reduce, refine) principle. Therefore, data from the control (empty) group, 1393-BG- and 0106-B1-BG-treated group have already been shown elsewhere in another context.[12]

2.4.2 Animals. Twenty-eight male, 12-week-old Sprague Dawley rats (Janvier, Le Genest St Isle, France) were used for the present study. Animals were held in groups in Macrolon type IV cages at a 12 h light/dark cycle at 22 ± 1 °C room air temperature with air humidity between 45–65%. Food pellets and tap water were provided *ad libitum*. The study was approved by the Animal Experimentation Ethics Committee of the Regierungspräsidium Karlsruhe (35-9785.81/G-269/18) and conducted following the European Union Directive (2010/63/EU) and institutional guidelines in the animal facility of the Heidelberg Orthopaedic University Hospital. The final analysis included n = 6 animals in the control group, n = 6 in the 1393-BG group, n = 7 in the 0106-B1-BG group and n = 6 in the 3-Zn-BG group. Three animals were lost due to post-operative complications.

2.4.3 Operative technique of intervention. Animals received a 4 mm defect on the femora of the left hind limb. Following the manufacturer's instructions, the osteotomy was performed with the RatFix 8-hole femoral plate system (RISystem, Davos, Switzerland). In short, animals received an injection of intraperitoneal anesthesia containing fentanyl (Panpharma, Trittau, Germany; 0.005 mg per kg body weight (BW)), medetomidine (Dormitor, Vétoquinol and Orion Pharma Animal Health, Lure, France; 0.15 mg per kg BW) and midazolam (Midazolam-hameln, hameln pharma, Hameln, Germany; 2 mg per kg BW). Antagonization post-operatively consisted of subcutaneous (sc.) injection of atipamezole (Revertor, cp-pharma, Burgdorf, Germany; 0.75 mg per kg BW) and flumazenil (Flumazenil Kabi, Fresenius Kabi, Bad Homburg, Germany; 0.2 mg per kg BW). After skin and fascia

incision, the bone was exposed by blunt separation of biceps femoris and vastus lateralis. On the anterolateral face of the femur, an 8-hole polyether ether ketone (PEEK) plate was applied and screwed tight by six screws. A standardized mid-diaphyseal femoral defect of 4 mm was set using a Gigli Wire Saw (RISystem). The defect was filled with scaffolds either consisting of 1393-BG, 0106-B1-BG or 3-Zn-BG. Prior to implantation, radiation with 30.0 Gy of the BG scaffolds took place. The control group consisted of empty defect sides. Muscular tissue, fascia and skin were sutured with resorbable material (Monosyn 5/0; B. Braun, Melsungen, Germany). For additional wound sealing, skin clips (AutoClip; Fine Science Tools, Heidelberg, Germany) were attached and removed after 7–10 days. Analgesia and antibiotics post-operatively consisted of sc. injection of buprenorphine (Buprenovet, Elanco, Bad Homburg, Germany; 0.05 mg per kg BW) every 12 h for 72 h and ampicillin (Ampi-Dry, veyx-Pharma, Schwarzenborn, Germany; 167 mg per kg BW) every 12 h for 48 h.

2.4.4 Evaluation and quantification of bone regeneration by μCT scanning. μCT scans were performed using a SkyScan 1076 (Bruker μCT, Kontich, Belgium). Specimens underwent *in vivo* scanning on D0 and D21 (1.0 aluminium filter, voltage of 65 kV, current 150 ms and 280 ms exposure time, frame averaging 2, rotation step 0.5°). Scans on D42 took place right after euthanasia with the same settings. D0 scans were performed immediately post-operative and anasthesia was antagonized after scanning. NRecon (Bruker μCT) was used for 3D-reconstruction, and bone defects were re-orientated using DataViewer (Bruker μCT). For qualitative evaluation of the defects, 3D images were generated with CT Vox (Bruker μCT). Thresholds were set as 60–200 to visualize the whole bone tissue containing less dense tissue and further dense tissue. To maintain a demarcation between the densities, the threshold for less dense tissue was set as 60–120 and for further dense tissue as 120–200.[21] Initial defect was defined as a region of interest (ROI) and transferred to D21 and D42. Five defect lengths in comparable intervals were measured between the two defect sides and an overall average was formed to relate the newly formed tissue to the length of the initial defect.

2.4.5 Histological analysis. Harvested specimens underwent PFA fixation (4% PFA in PBS), decalcification, and embedment in paraffin,[12,22–24] and five longitudinal slices of 5 μm of the visible defect were cut (pfm Rotary 3006 EM, PFM medical, Cologne, Germany). Staining with Movat's pentachrome (MVP) was performed for qualitative and quantitative assessment of osteoid and chondrogenic tissue at the defect side, following previously described protocols.[25–27] Low calcified tissue took on dark orange, high calcified tissue bright yellow, and non-mineralized chondrogenic tissue green colour.[24,28,29] For further assessment of the osteogenic development of the newly formed tissue, cells with resorptive activity, such as osteoclasts were visualized using TRAP staining.[30,31] Vascular structures were analysed using the IgG_1 PECAM-1 antibody (sc-376764; Santa Cruz Biotechnology, Heidelberg, Germany), which binds specifically to platelet endothelial cell adhesion molecule-1 (PECAM-1) or CD31. Antibody was diluted 1 : 200 in 1% goat serum (Dako, Glostrup, Denmark) as previously described.[28] ImageJ software was used for quantification of bone regeneration by MVP, osteoclasts by TRAP and vascularization by CD31 staining as described previously.[12]

2.5 Statistics

IBM SPSS (Version 25; IBM, Armonk, NY, USA) was used for statistical analysis. Statistically significant parameters in the Kruskal–Wallis multigroup test were further analyzed for significance between individual groups using the Mann–Whitney *U* test. Statistically significant differences at $p \leq 0.05$. No correction for multiple testing was performed due to the exploratory design of the study.[32] GraphPad Prism (Version 9.3.1; GraphPad Software, La Jolla, CA, USA) was used to design graphs.

3 Results

3.1 BG characterization

3.1.1 Crystallinity of BGs and morphology of BG scaffolds. The Zn-doped borosilicate 0106-B1-BGs demonstrated an amorphous structure before and after the sintering process, as depicted in Fig. 1A. Moreover, the characteristic values of particle size distribution are shown in Fig. 1B, showing no significant differences between BG compositions. Regarding the produced scaffolds, Fig. 1C shows a highly porous structure characteristic of foam replica-derived scaffolds.[4,5] There were no significant morphologic differences detected between the three BG compositions. The scaffolds showed a pore diameter range of 200–600 μm. Similar results were reported for the reference 0106-B1-BG scaffolds.[12] Additionally, the Zn-containing BG scaffolds showed a slight superior compressive strength compared to the reference 0106-B1-BG scaffolds (Fig. 1D).

3.1.2 Ion release profiles. 3-Zn-BG showed the highest release of silicon ions, while 0106-B1-BG and 2-Zn-BG showed similar behaviour (Fig. 2A). Moreover, after the third day of incubation, silicon release was slower for 1-Zn-BG compared to the other BGs; this trend was observed within the first 14 days of incubation. The release of phosphate from 0106-B1-BG was below the level of the Zn-BGs at all time points (Fig. 2B). In terms of release of calcium ions, there was a clear trend difference between the reference BG and the Zn-containing compositions (Fig. 2C). The maximum release of Ca^{2+} from the 0106-B1-BG occurred at 1 day of incubation, whereas for the Zn containing glasses the release lasted until 7 days of incubation, reaching maximum values at 3 days of incubation. The BG composition with higher release of Ca^{2+} was 1-Zn-BG, which was the BG composition with the lowest substitution of CaO by ZnO, leading to higher Ca^{2+}/Zn^{2+} release ratios followed by 2-Zn-BG and 3-Zn-BG. 0106-B1-BG showed the fastest release of boron (B^{3+}) (Fig. 2D), while zinc (Zn^{2+}) release increased with higher Zn content in the Zn-BGs (Fig. 2E).

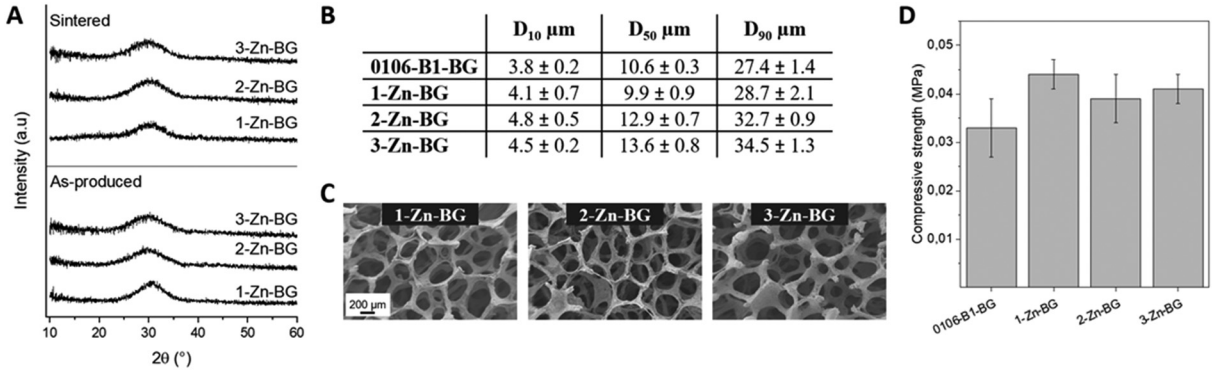

	D_{10} μm	D_{50} μm	D_{90} μm
0106-B1-BG	3.8 ± 0.2	10.6 ± 0.3	27.4 ± 1.4
1-Zn-BG	4.1 ± 0.7	9.9 ± 0.9	28.7 ± 2.1
2-Zn-BG	4.8 ± 0.5	12.9 ± 0.7	32.7 ± 0.9
3-Zn-BG	4.5 ± 0.2	13.6 ± 0.8	34.5 ± 1.3

Fig. 1 Characterization of BGs. (A) X-ray diffractograms of produced and sintered particles. (B) Particle size distribution of sintered BGs. (C) SEM micrographs of BG scaffolds. (D) Compressive strength of BG scaffolds.

3.2 *In vitro* results

3.2.1 Cell quantification and viability in direct co-culture with BGs. Significantly higher cell numbers for all Zn-BG groups on D7 and D21 were observed compared to 0106-B1-BG (Fig. 3A). Additionally, on D21 the 1-Zn-BG group showed significantly higher cell numbers in comparison to 3-Zn-BG. Cell viability was significantly increased by 1-Zn-BG on D7. On D21, the presence of all Zn-BGs increased the cell viability in comparison to the 0106-B1-BG (Fig. 3B). Increased viability was detected for BMSCs cultivated with 2-Zn-BGs on D21.

BMSCs showed the typical spindle-shaped appearance in all groups (Fig. 3C). On D7, cell density appeared to be the lowest in the 0106-B1-BG group. This matched the results in the cell quantification by DAPI.

3.2.2 Influence of the BGs on osteogenic differentiation of BMSCs. mRNA expression levels of ALP were not significantly affected when comparing the different BGs on D7 (Fig. 4A). On D21, 2-Zn-BG significantly increased ALP mRNA expression in comparison to the 1-Zn-BG group. Significantly higher ALP activity was detected in the 1-Zn-BG group on D7 (Fig. 4B). Exposure to 2-Zn-BG led to a significant increase in ALP activity compared to 3-Zn-BG and 0106-B1-BG on D21.

For OPN, no significant differences in mRNA expression levels on D7 were found, and 2-Zn-BG induced a significantly higher level of OPN on D21. 3-Zn-BG induced the highest level of OPN protein production on D7 (Fig. 4D). On D21, higher OPN concentrations in the supernatants of 2-Zn and 3-Zn-BG groups were measured compared to the 0106-B1-BG group. The highest overall OPN protein concentration was found on D21 in the 3-Zn-BG group. On D7, OCN mRNA expression did not show significant differences amongst the groups (Fig. 4E). On D21, however, the presence of the Zn-BGs led to an increase in OCN mRNA levels compared to 0106-B1-BG. COL1A1 mRNA levels were significantly higher for 2-Zn-BG and 3-Zn-BG compared to 0106-B1-BG on D7 (Fig. 4F). Furthermore, COL1A1 mRNA levels of 3-Zn-BG significantly exceeded those of 1-Zn-BG. On D21, similar observations could be made. Additionally, higher COL1A1 mRNA levels in the 2-Zn-BG groups were measured compared to the 1-Zn-BG group.

3.2.3 Angiogenic properties of the BGs. On D7, higher levels of VEGF mRNA in the 3-Zn-BG group were detected in comparison to the 0106-B1-BG group (Fig. 5A). On D21, VEGF mRNA levels in the 2-Zn-BG group significantly surpassed those of the other Zn-BGs. The VEGF protein presence between the groups did not differ on D7 (Fig. 5B). On D21, particularly higher VEGF protein content was measured in the 1-Zn-BG group in comparison to the 3-Zn-BG group. For PlGF, on D7, no significant differences of the mRNA levels were observed between the groups (Fig. 5C). On D21, PIGF mRNA expression was reduced in presence of 1-Zn-BG compared to 0106-B1-BG and 2-Zn-BG. Significantly higher PlGF protein levels were detected in the Zn-BG groups in comparison to 0106-B1-BG on D7 (Fig. 5D). PlGF protein levels increased with increasing Zn content amongst the Zn-BGs on D21. On D7 and D21, no significant differences in EDN1 mRNA expression were detected between the groups (Fig. 5E). However, EDN1 protein levels were increased by the presence of 3-Zn-BG compared to 2-Zn-BG on D7 (Fig. 5F). Protein contents significantly increased by all Zn-containing BGs compared to 0106-B1-BG. On D21, 2-Zn-BG and 3-Zn-BG showed increased EDN1 protein levels compared to 0106-B1-BG.

3.2.4 Influence of the BGs on HUVEC-mediated tube network formation. Qualitative analysis of the HUVECs network formation revealed a developed network in the M200 group (Fig. 6A). The network of the 0106-B1-BG group was slightly disrupted, not as much as in the control group without supplements. The Zn-BG groups formed a continuous network compared to 0106-B1-BG. A significantly higher number of junctions was detected in the Zn-BG groups in comparison to 0106-B1-BG (Fig. 6B). A significantly higher number of junctions was found for the 2-Zn and the 3-Zn-BG groups in comparison to the 1-Zn-BG group, with a gradual increase of this parameter from the lowest to the highest Zn portion. Similar observations were made for the total master segment lengths (Fig. 6C).

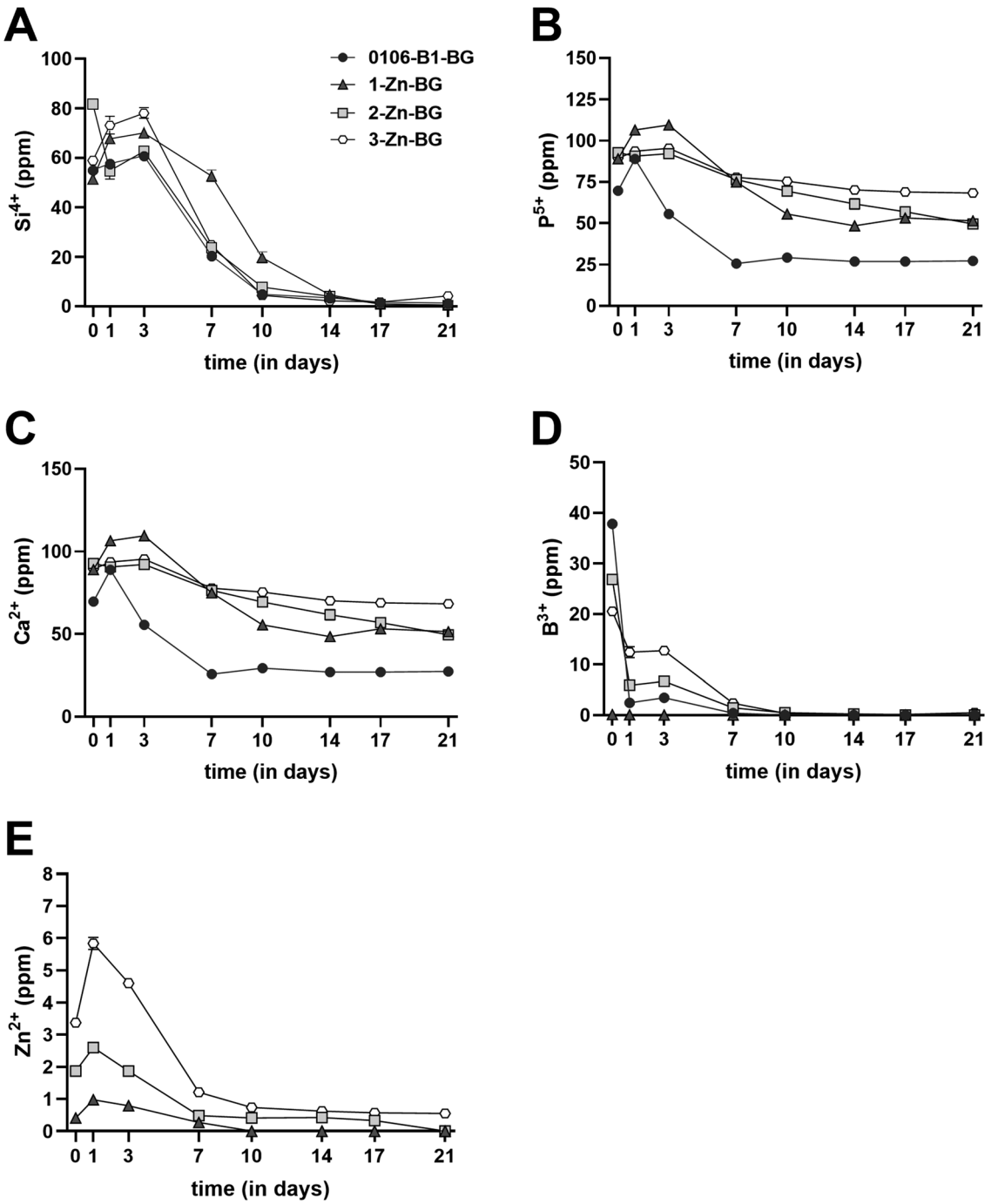

Fig. 2 Ion release profiles of 0106-B1-BG and the Zn-BGs. Measurement of ion release by inductively coupled plasma optical emission spectrometry (ICP-OES). Release in ppm of silicon (Si^{4+}) (A), phosphate (P^{5+}) (B), calcium (Ca^{2+}) (C), boron (B^{3+}) (D) and zinc (Zn^{2+}) (E) ions in DMEM. Day 0 corresponds to ion release measurement after the preconditioning period of the BGs (24 h in DMEM), from day 1, the measurements directly correspond with the incubation time in the cell culture studies.

3.3 *In vivo* results

3.3.1 Qualitative and quantitative μCT analysis of new tissue growth. In the chosen observation period, no full defect bridging was achieved in any group, as shown by qualitative analysis of μCT images (Fig. 7).

From D0 to D21, almost complete scaffold degradation in the 0106-B1-BG and 3-Zn-BG group was observed. In the 1393-BG group scaffolds was still clearly visible after this time. A higher volume of less dense tissue was detected for all intervention groups compared to the empty defect on D21 (Fig. 8A). For the 1393-BG group higher volume of less dense tissue in contrast to the other BG groups was detected at D21 and D42 (Fig. 8B). Significant differences were found for the volume of further dense tissue between the 1393-BG group and all other

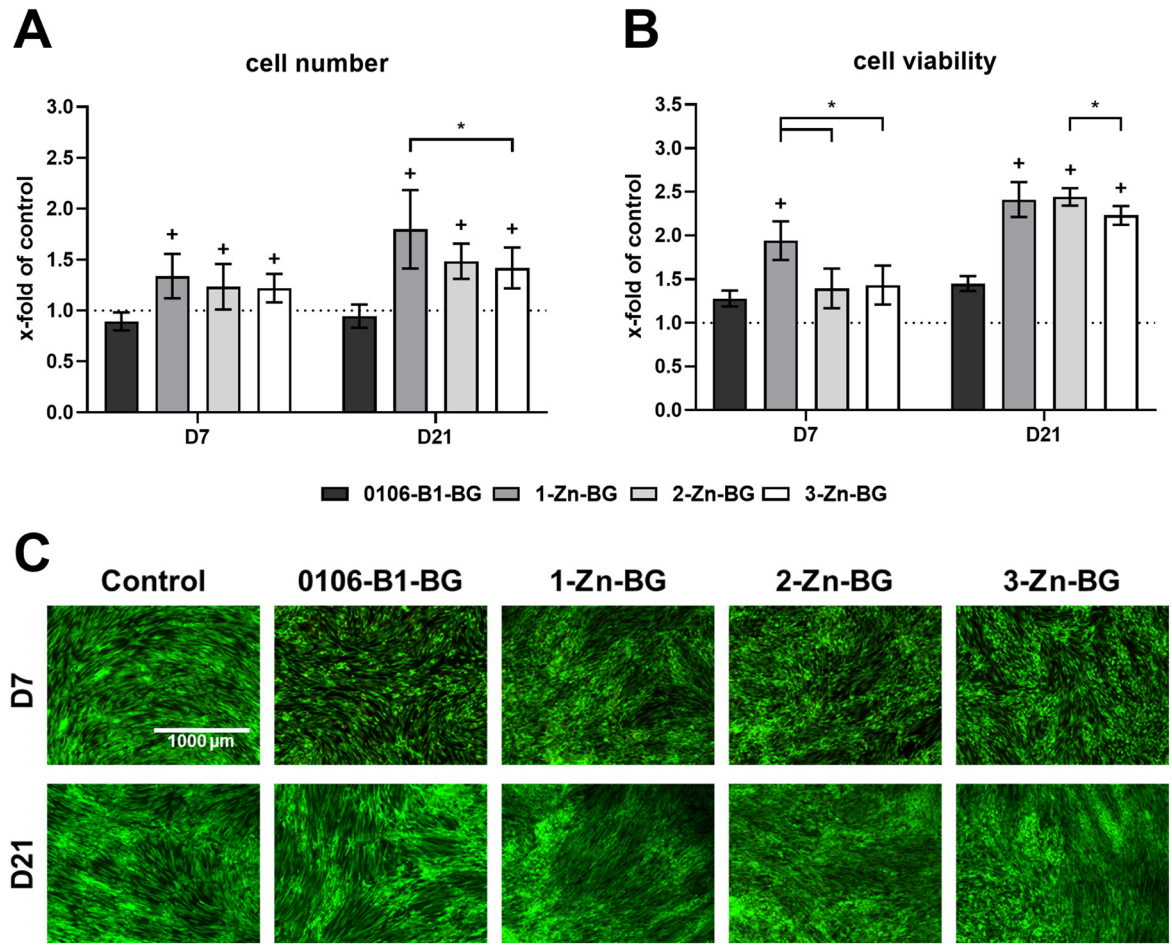

Fig. 3 Cell number and viability. BMSCs were cultivated in direct contact with 1 mg ml^{-1} 0106-B1, 1-Zn, 2-Zn and 3-Zn-BG for the indicated time points. The control group was cultured in CCM. Cell number (A) was quantified by DAPI fluorescence intensity (FI), and cell viability (B) was quantified by FDA FI. Differences between the Zn-BG groups and 0106-B1-BG are indicated by (+), between the Zn-BG groups, represented by the brackets, are indicated by (*). Cell viability and morphology in cell culture setting were visualized by FDA/PI staining (C). Scale bar refers to 1000 µm and applies to all images.

groups on D21 (Fig. 8B). The groups with 0106-B1-BG and 3-Zn-BG scaffolds showed a significantly larger defect closure on D21 in comparison to the control group and to the 1393-BG group (Fig. 8C).

3.3.2 Histological assessment of bone formation. For the empty defect and the defect filled with the BGs, typical aspects of the woven bone were detected (Fig. 9A). Fibrous tissue was also visible in the defect side of all experimental groups. The area in the defect with newly formed bone was quantified by MVP staining. Higher bone formation was assessed in the 0106-B1-BG group compared to the defects left empty (Fig. 9B). For defects treated with 3-Zn-BG higher bone formation was detected compared to the control group and the 1393-BG group.

TRAP-positive areas were detected at the interface between the defect ends and the area of newly formed tissue in all groups (Fig. 10A). In the central part of the BG-treated defects, TRAP-positive areas were detected. The defect of 0106-B1-BG showed larger continuous TRAP-positive structures compared to the other defects. Quantification revealed a significantly increased presence of TRAP-positive areas in defects treated with 0106-B1-BG in comparison to the control, the 1393-BG and the 3-Zn-BG groups (Fig. 10B). A significantly higher TRAP-positive area was found in the defects treated with 3-Zn-BG compared to the control.

CD31-positive structures were detected at the interface between the defect ends and the area of newly formed tissue in all groups (Fig. 11A). For the BGs, CD31-positive structures were also visible in the central aspects of the defect site. The CD31-positive area was numerically larger in the 0106-B1-BG and the 3-Zn-BG group in comparison to the control and the 1393-BG group (Fig. 11B).

4 Discussion

In recent years, the targeted adaptation of BG compositions by incorporating biologically active ions has become an impor-

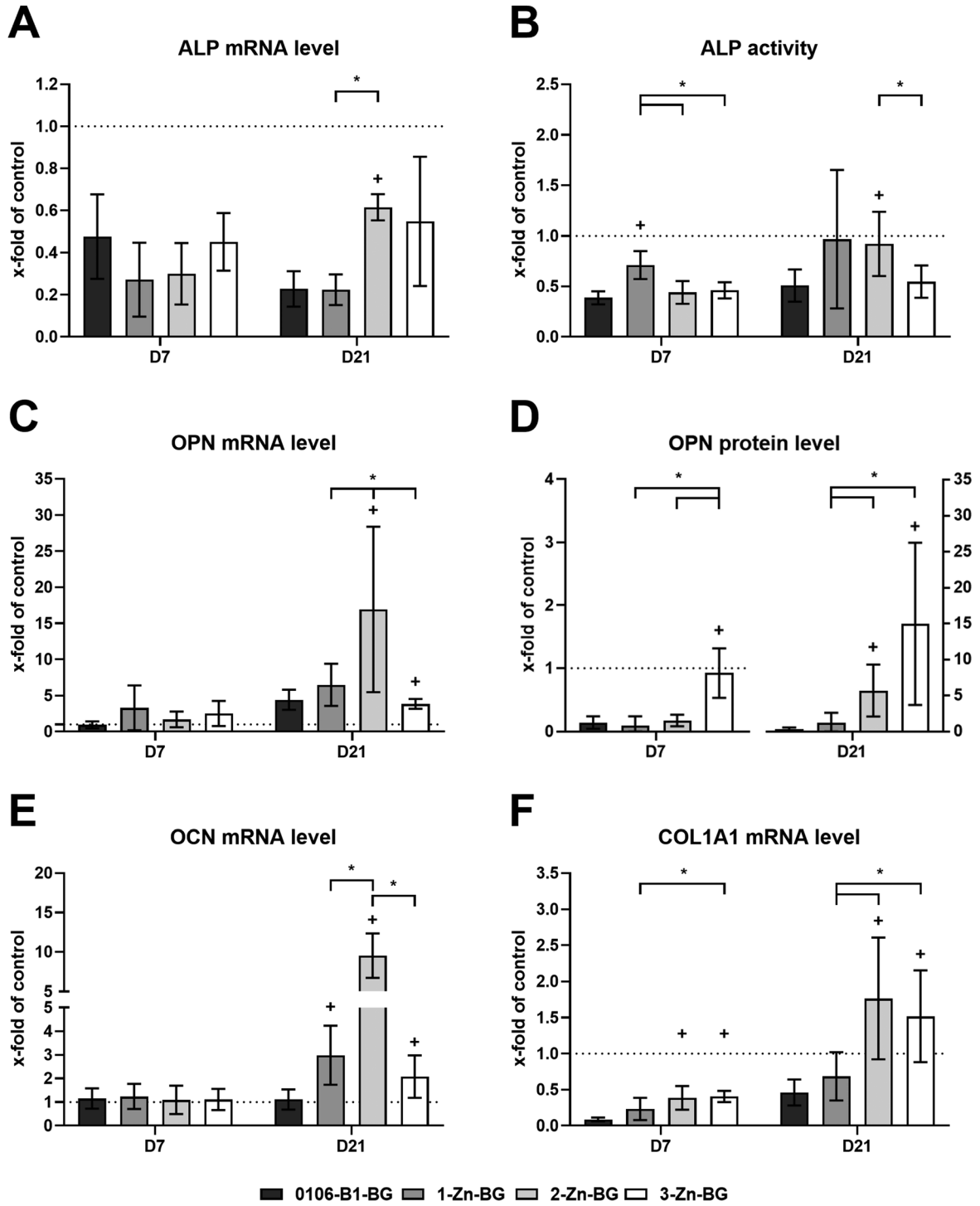

Fig. 4 Osteogenic differentiation of BMSCs. Influence of the 0106-B1, 1-Zn, 2-Zn, and 3-Zn-BG on osteogenic differentiation, measured on mRNA and protein level on D7 and D21. ALP was measured on mRNA level (A) as well as on the activity level (B). OPN was analyzed on mRNA level (C) and on protein level (D), left axis refers to D7, right axis to D21. OCN (E) and COL1A1 (F) were analyzed on mRNA level. Differences between the Zn-BG groups and 0106-B1-BG are indicated by (+), and between the Zn-BG groups, represented by the brackets, are indicated by (*).

tant task of BG development and BG-focused research.[33] By incorporating ions with known biological effects, BGs can be tailored towards their anticipated field of use: for example, the borosilicate 0106-B1-BG composition has already demonstrated encouraging characteristics in bone tissue engineering approaches due to a B-mediated stimulation of angiogenic response and, consequently, enhanced osteogenic properties compared to B-free BG compositions.[8,9,12,28] In the present

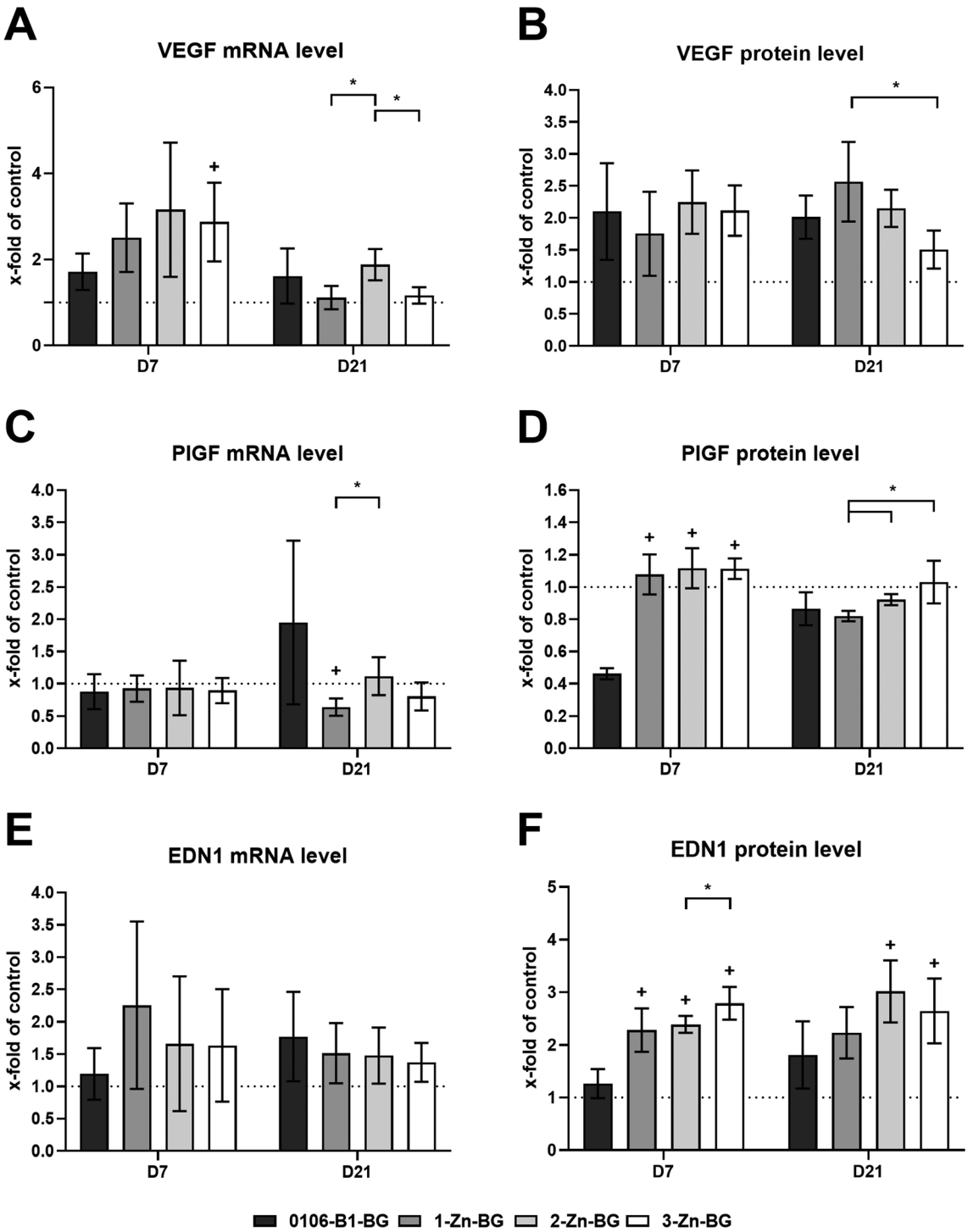

Fig. 5 Angiogenic properties of the BGs. Influence of the 0106-B1, 1-Zn, 2-Zn and 3-Zn-BG on angiogenic markers on mRNA and protein level. On D7 and D21, mRNA levels and protein concentrations of VEGF (A and B), PlGF (C and D) and EDN1 (E and F) were evaluated. Differences between the Zn-BG groups and 0106-B1-BG are indicated by (+), and between the Zn-BG groups, represented by the brackets, are indicated by (*).

study, Zn was added to the 0106-B1-BG composition in order to enhance its osteogenic properties further since Zn is known to stimulate bone formation by various mechanisms such as the regulation of osteoblastic differentiation markers like ALP, COL1A1, OPN or OCN.[14,15] Zn was added in increasing portions to the basic 0106-B1-BG in exchange for CaO, resulting in three new BG compositions, namely 1-Zn, 2-Zn, and 3-Zn-BGs, which were comparatively examined in this study.

A positive influence of the Zn-BGs on cell viability and growth was shown. The increased viability could be caused by

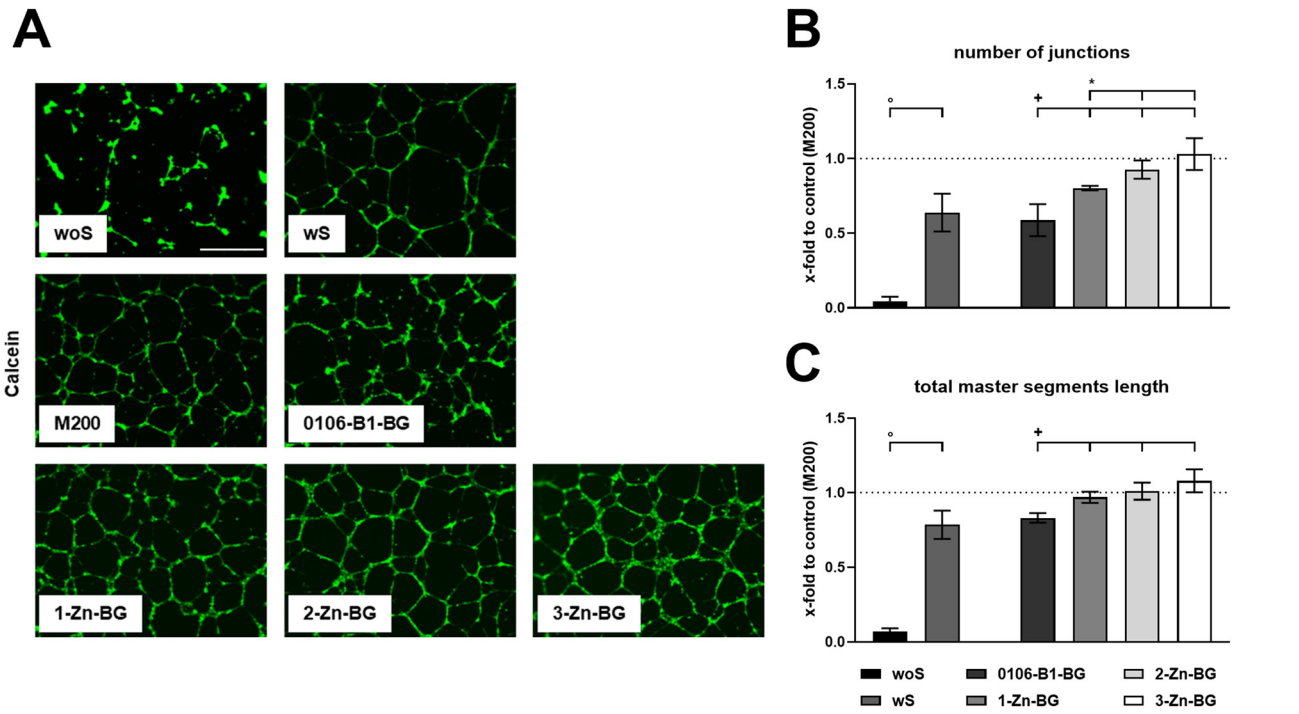

Fig. 6 Influence of the BGs on HUVEC-mediated tube network formation. (A) Representative fluorescent images showing the formation of tubular networks by HUVECs within the different groups. Scale bar = 1000 μm. woS = without supplements; wS = with supplements. Quantification of (B) number of junctions and (C) total master segments length. All values were normalized to the M200 control group, shown as the dotted line. (°) marks significant differences compared to woS, (+) marks significant differences to 0106-B1-BG, and (*) marks significant differences between the Zn-BGs as indicated by the brackets.

the different ion release kinetics of the BGs. Here, Zn-BGs showed an increased release of Si, which has a concentration-dependent effect on cell proliferation.[33,34] However, with the increasing presence of Zn, cell viability was reduced. Similar findings were reported in other studies where increasing Zn content in BGs resulted in lower biocompatibility.[35,36] A study by our group showed a negative correlation between the concentration of Zn-doped MBGNs and cell viability.[16] Doping of BGs based on the 58-S composition by replacing CaO with 1, 5, and 10 mol% ZnO resulted in increased cytotoxicity, depending on the concentration, and decreased bioactivity with respect to the formation of an apatite layer.[37] In the present study, the release of Zn from the BGs peaked early at D1; for 1-Zn-BG, a concentration of Zn ions of 15 nM, for 2-Zn-BG of 40 nM and 3-Zn-BG of 90 nM could be detected, decreasing until D10 to a constant level ranging from nearly 0 nM to 12 nM between the Zn-BGs. In parallel, with ongoing incubation time, the Zn-BGs positively influenced the cell viability and cell number. This might be attributed to the decreased release of Zn: $ZnCl_2$ has been shown to enhance the viability of human umbilical cord-derived mesenchymal stem cells in a certain concentration range, while at higher concentrations, negative effects of $ZnCl_2$ on cell viability were reported.[38] This concentration was not reached in the present study, and therefore, the positive dose-dependent effect of Zn on the viability could be confirmed.

Zn showed a positive effect on the osteogenic potential of the BGs *in vitro*. However, the effects of Zn concentration on osteogenic differentiation of BMSCs were variable. For example, 1-Zn-BG at D7 and 2-Zn-BG at D21 showed increased activity of ALP. For OPN, 2-Zn-BG increased mRNA and protein expression of BMSCs at D21, and 3-Zn-BG showed increased OPN protein levels at D7 and D21. OCN mRNA expression levels at D21 were higher for all Zn-BGs compared to the 0106-B1-BG, and COL1A1 mRNA expression was increased by BMSCs cultivated in the presence of 2-Zn and 3-Zn-BG. It has been reported that ALP activity is induced by Zn,[15,39–41] and Zn deficiency results in lower activity in osteoblasts and, thus, reduced mineralization.[39,42] Increased production of OCN can also be induced by Zn.[40,43] Release of Zn was highest at the 3-Zn-BG during all time points. None of the Zn-BGs in our study dominated all osteogenic markers, so it can be assumed that the optimal concentration of Zn for inducing expression varies between genes. In a study by Yusa *et al.*,[44] 0.32 nM, 3.2 nM and 32 nM Zn ions were eluted from Zn-modified titanium. Increased gene expression of COL1A1, OCN, and ALP was detected when incubated for 7 days with 3.2 nM Zn ions.[44] In our study, Zn ion concentrations of 5 nM could be measured for the 2-Zn-BG from day 7 on but showed their effect later by higher mRNA expression levels of ALP, OPN, OCN, and COL1A1 on D21, and the effect decreased for OCN and OPN at higher concentrations. A 5 wt% Zn-containing borosilicate glass was shown to result in a higher ALP concentration of incubated BMSCs in comparison to more and less Zn-containing glasses, indicating that the 5 wt% Zn glass pro-

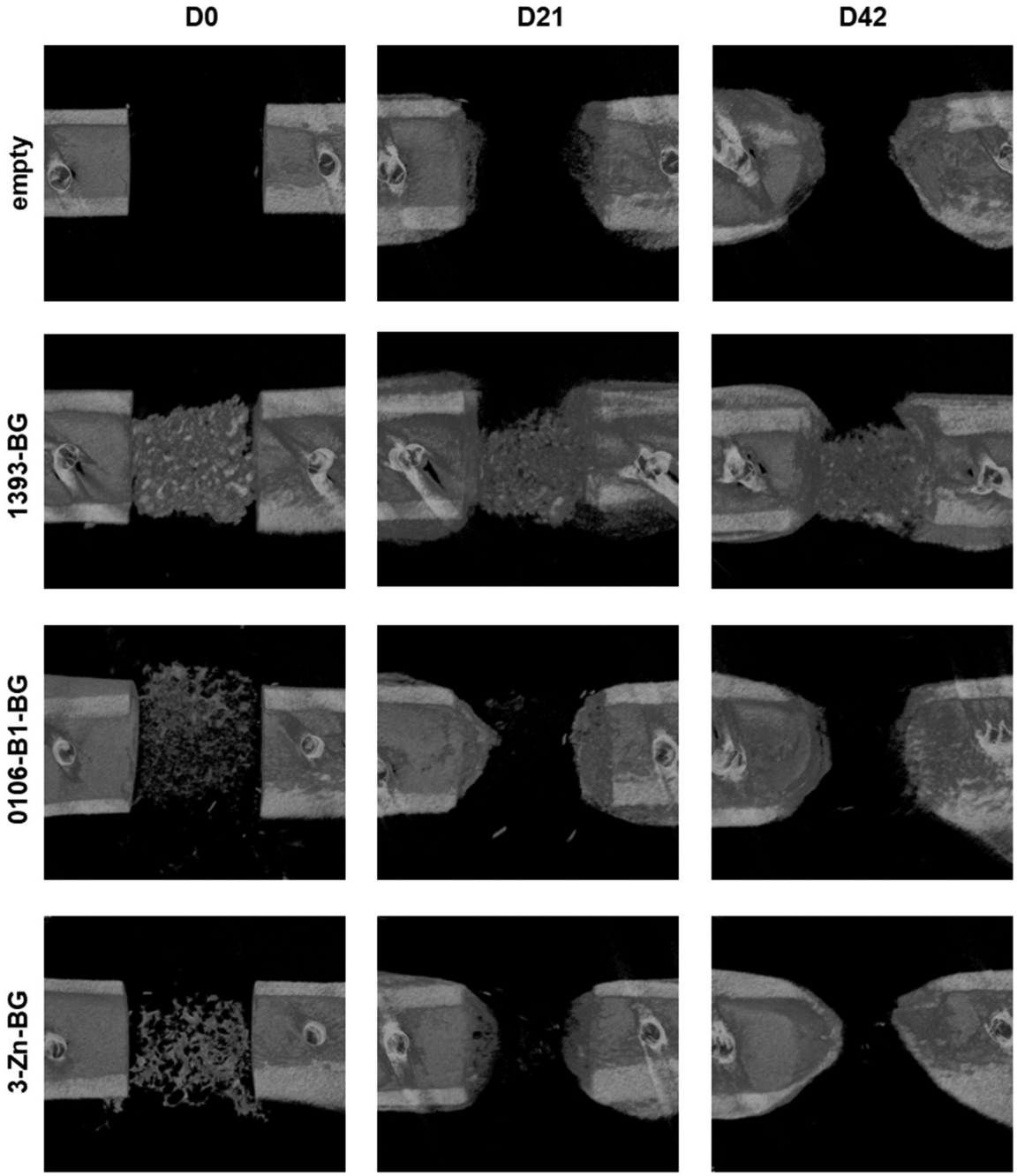

Fig. 7 Qualitative μCT analysis of new tissue growth. *In vivo* tissue formation in empty and BG-filled defect sites. Representative pictures of μCT scans at D0, D21 and D42, overall grayscale threshold of 60–200.

motes differentiation of BMSCs.[36] MBGNs doped with Zn showed pro-osteogenic properties of BMSCs through increased expression of the osteogenic differentiation genes ALP, OPN, and COL1A1.[16] Comparing these with our data, the 3-Zn-BG, containing 5 wt% Zn, showed a good performance for the expression of COL1A1 and OPN, but did not show increased levels of ALP. Si plays an important role and can lead to increased expression of COL1A1, ALP, and OCN.[33] In our study, an increased release of Si was shown for 1–Zn and 3-Zn-BGs at D1 and D3. Boron also has an effect on osteogenic differentiation and showed concentration-dependent expression of osteogenic differentiation markers of ALP, OCN, and COL1A1 and ALP activity after 7 days of cultivation.[45–47] In our study, 1-Zn-BG showed almost no release of B, 3-Zn-BG showed the highest release from D1, followed by 2-Zn-BG and 0106-B1-BG at D7 and D21, which is mainly relevant for osteogenic differentiation.[48] Since no additional stimuli were used, the observed effects on the expression levels of BGs were ascribed

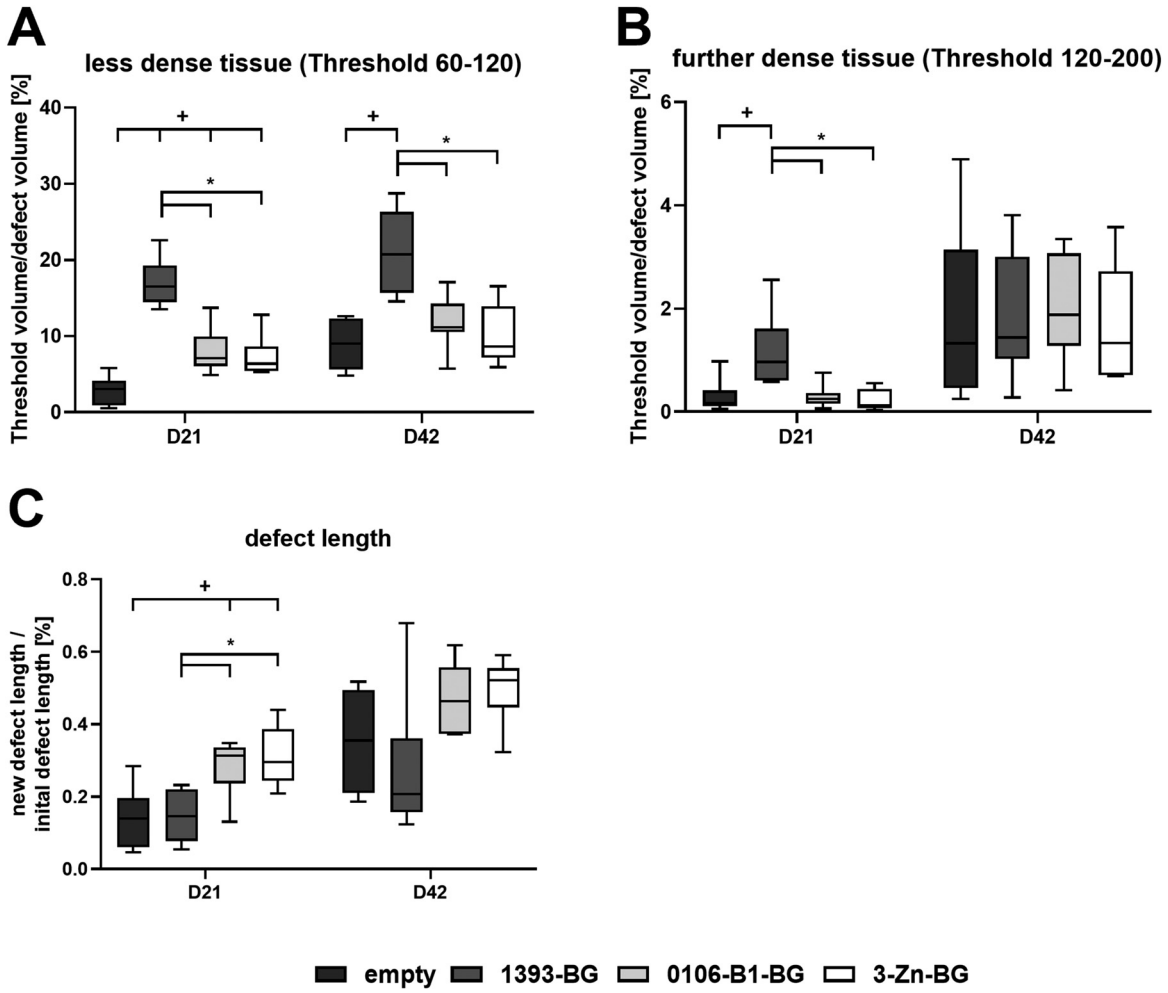

Fig. 8 Quantitative μCT analysis of defect sites. Quantification of threshold volume of less dense (A) and further dense (B) tissue for D21 and D42 in relation to defect volume. Quantification of the initial defect closure (C) for the different groups. Differences between BG groups and the control group are indicated by (+), between 1393-BG, 3-Zn-BG and 0106-B1-BG by (*).

to the direct contact of BMSCs and BGs and their ionic dissolution products.[49] It can be assumed that the defined composition of the BGs and the ions besides Zn[8,33] have a combined interaction on the osteogenic differentiation of BMSCs.

The angiogenic potential was positively affected by the presence of Zn. PlGF protein level was increased at D7 for all Zn-BGs, especially for the 3-Zn-BG at D21. EDN1 protein was highly expressed by 2-Zn- and 3-Zn-BGs at both time points. A continuous network of HUVECs was observed for all Zn-BGs, which even showed a significantly higher number of junctions and increased total master segment length compared to the 0106-B1-BG. Zn has been shown to influence the expression of angiogenic markers. For example, a study based on 5% Zn-containing 45S5-BG demonstrated a promoting effect on endothelial cell adhesion.[50] Cultivation of BMSCs with 10 μM Zn results in increased release of VEGF,[51] while co-cultivation of HUVECs with Zn implanted titanium plates has been also reported.[52] Interestingly, enhanced migration and formation of capillary-like structures were observed in HUVECs in the presence of EDN1,[53] which suggests a connection between EDN1 and tube formation by HUVECs. This behavior is reflected in our results as the Zn-BGs showed high expression of EDN1 as well as good performance in the tube formation assay. In another study HUVECs cultured in the presence of human mesenchymal stem cells on scaffolds of 1 and 2 wt% ZnO showed enhanced angiogenic behavior.[54] It has been shown that at high Zn concentrations of 140 μM, the expression of EDN1 in endothelial cells is increased, whereas at a lower concentration (60 μM), the angiogenic behaviour tended to be downregulated overall.[55] It is then confirmed that the angiogenic effect of Zn is strongly dependent on its concentration.[33] This is in agreement with our findings, where 3-Zn-BG with releasing a peak concentration of 90 nM, showed overall the best performance in the angiogenic gene expression as well as in the tube formation assay.

The 3-Zn-BG composition presented itself positively in terms of cytocompatibility and osteogenic protein expression

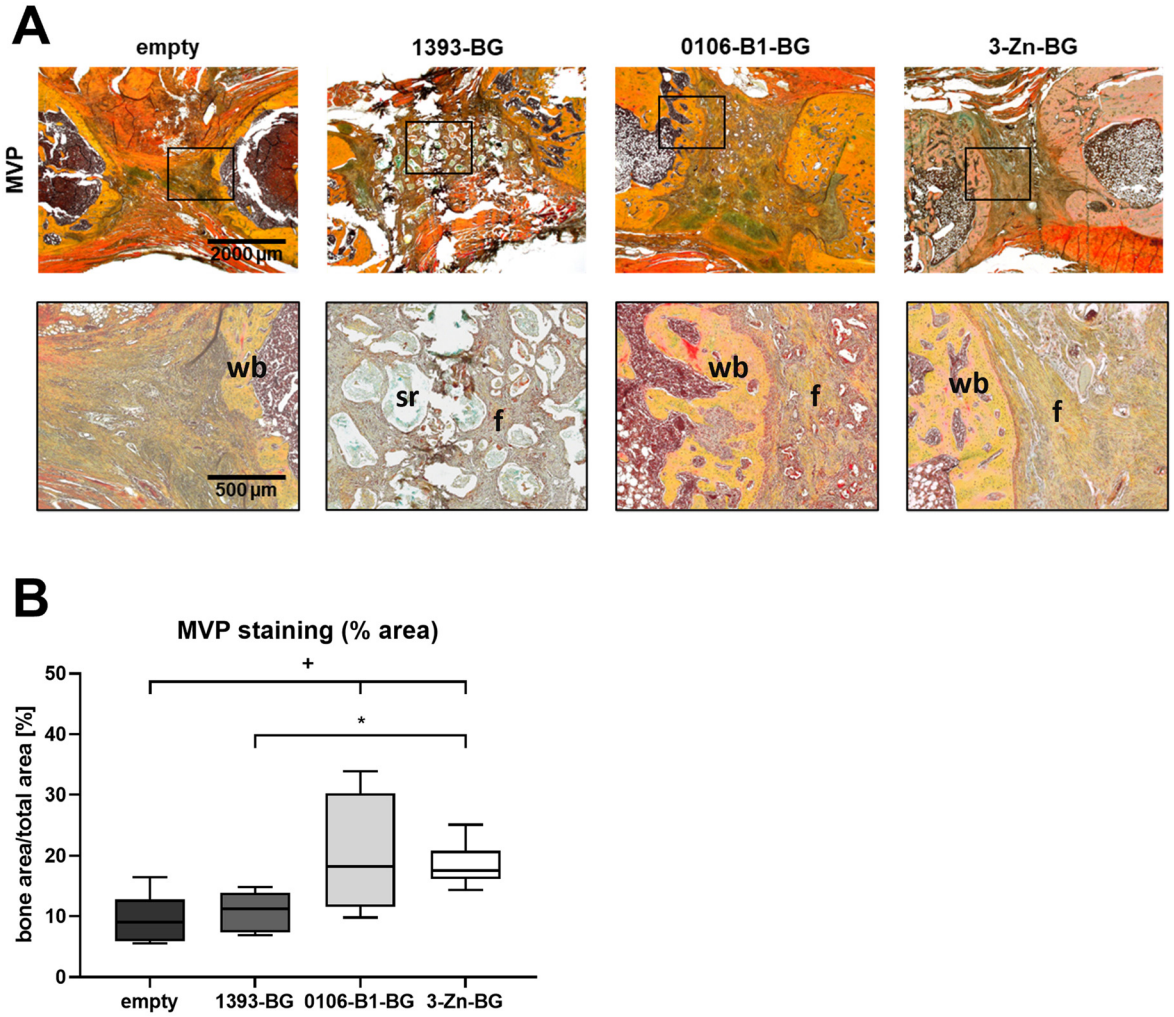

Fig. 9 Histological overview and analysis of bone formation. Histological evaluation of bone formation in the defects by qualitative (A) assessment by MVP staining on D42. Scale bars refer to 2000 µm or 500 µm, as indicated. f = fibrous tissue, wb = woven bone, sr = scaffold remnants. Representative pictures are shown. Quantitative evaluation of newly developed bone area within the defect sites (B). Differences between BG groups and control group are indicated by (+), between 1393-BG, 3-Zn-BG and 0106-B1-BG by (*).

and showed a positive influence on *in vitro* angiogenic response of BMSCs as well as on tube formation by HUVECs. Therefore, it was chosen to be evaluated within the *in vivo* part of the study.

Prior to the implantation of the scaffolds, gamma irradiation was performed for sterilization purposes. This has already been done for the 1393-BG and the 0106-B1-BG scaffolds in previous studies and showed no limitations regarding the *in vivo* performance.[12,28] A reduction of the defect length, as well as new bone formation and an increase of the bone surface, could be observed 42 days after implantation of the scaffolds into the critical-size defect. Due to the contact with body fluids and the biological processes taking place, only small residues of the BG scaffolds could be detected in the defects after this time, which represents the expected degradation of the scaffolds *in vivo*. Lengths of the defects filled with 0106-B1-BG and 3-Zn-BG scaffolds shortened 21 days after implantation compared to the untreated defect and the 1393-BG group, and more of a less dense tissue could be detected, which indicates an accelerated bone regeneration potential. This effect is lost after 42 days; although the defect distances are further shortened, they no longer show any differences between the groups. After 42 days, no difference in defect length could be detected, but denser tissue was observed for all groups, representing remodelling to mature bone tissue.[21,56] µCT assessment, however, allows a differentiation between the density of tissue. Thus, the indicated thresholds only allow for an indirect assumption about the type of tissue that is shown. The group filled with 1393-BG showed higher amounts of less and more dense tissue, which in combination with the visual evaluation of the µCT images may be due to the large amount of remaining scaffolds. In order to enable a specific tissue detection, histological staining of the specimens was performed. The MVP staining confirmed enhanced bone formation in 0106-B1-BG in comparison to the empty defect and for the 3-Zn-BG additionally in comparison

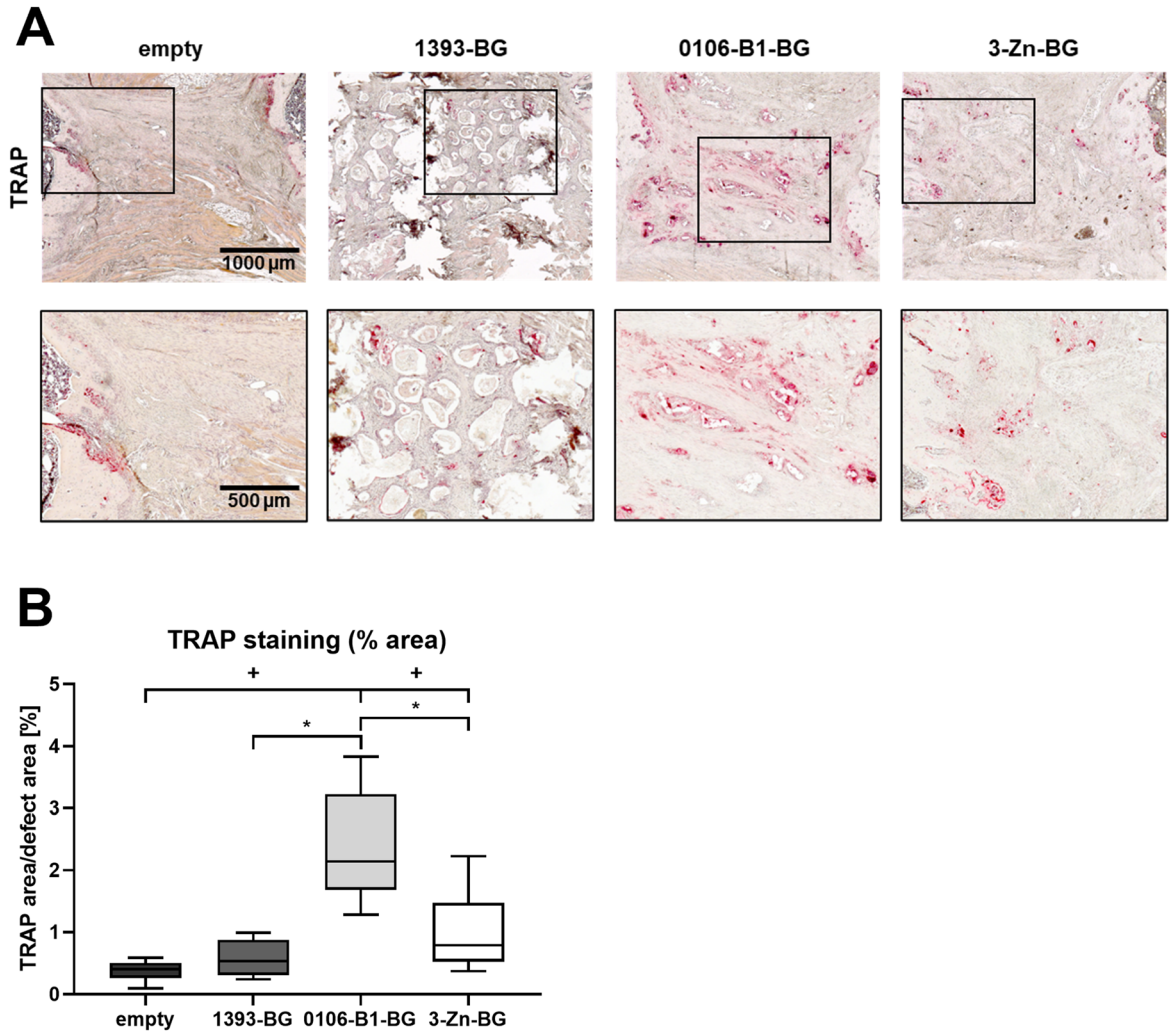

Fig. 10 Histological overview and analysis of bone formation. Histological evaluation of bone formation in the defects by qualitative (A) assessment by MVP staining on D42. Scale bars refer to 1000 µm or 500 µm, as indicated. Representative pictures are shown. Quantitative evaluation of TRAP-positive area (B) to defect area. Differences between BG groups and the control group are indicated by (+), between 1393-BG, 3-Zn-BG and 0106-B1-BG by (*).

to the 1393-BG, confirming the osteo-regenerative potential of the BG scaffolds. Zn-containing BG scaffolds showed a slight superior compressive strength compared to the reference 0106-B1-BG scaffolds. These results are in agreement with values found in the literature for similar borosilicate BG scaffolds produced *via* the foam replica technique in the range of 0.04 MPa, as well as for 45S5-BG scaffolds prepared by the same method (0.3–0.4 MPa).[5]

In a previous study by our research group, 0106-B1-BG was shown to have a comparable osteo-regenerative potential to scaffolds made of 45S5-BG in an ectopic model.[12] According to our evaluation, the 3-Zn-BG has a similar effect on bone regeneration to 0106-B1-BG. When a Zn-containing 45S5-BG was implanted into rat muscle tissue, the presence of multiple vessels and increased ALP activity were detected. This indicates a pro-osteogenic environment of the Zn-containing BG.[57] In another previous study, a 5 wt% Zn borosilicate glass based on the 1393-B2-BG composition was implanted into calvaria defects in rats; 8 weeks after implantation, the Zn-containing BG showed significantly better bone regeneration compared to the undoped control group.[36] However, only limited evidence about the *in vivo* performance of Zn-containing BGs is available.[39]

Osteoclasts have a key role in the remodelling of provisional bone to mature bone.[58] TRAP staining demonstrated increased activity of osteoclasts in the defects with implanted 0106-B1-BG and 3-Zn-BG scaffolds, compared to the untreated defect. At the same time, 0106-B1-BG showed increased TRAP presence compared with the 1393-BG and the 3-Zn-BG. In the 0106-B1-BG and the 3-Zn-BG groups, osteoclasts were detected mostly in the bone-to-defect transition area, as well as in the area of the remaining scaffold remnants. In addition to active bone remodelling, this result also indicates that the remaining scaffold remnants are actively degraded by osteoclasts. This be-

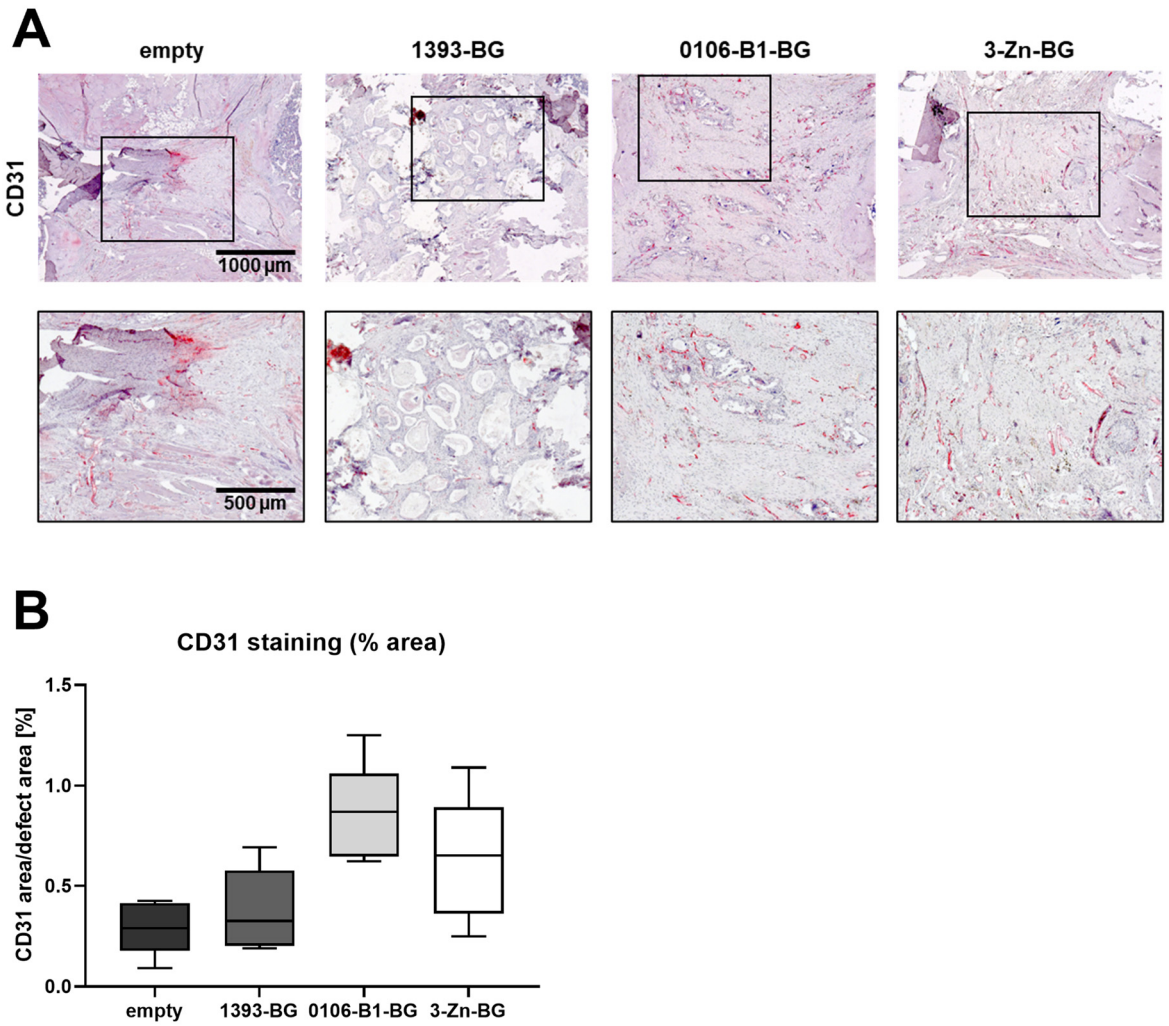

Fig. 11 Analysing vascular structures. Qualitative assessment of CD31 positive areas (A) in the defect site. CD31 positive cells are shown in bright red. Scale bars refer to 1000 µm or 500 µm, as indicated. Representative pictures are shown. Quantitative evaluation of CD31-positive area (B) to defect area. Differences between BG groups and the control group are indicated by (+), between 1393-BG, 3-Zn-BG and 0106-B1-BG by (*).

havior has also been observed in other studies.[12,59] When scaffolds made out of Biosilicate BG with two crystalline phases were implanted into calvaria defects in rats, osteoclasts could be stained, especially at the interface between bone and defect and around the remaining BG remnants using TRAP.[59] In a study of our group, scaffolds made of a β-tricalcium phosphate-based bone substitute (Vitoss) and Vitoss BA, which is additionally supplemented with 20 wt% 45S5-BG particles, were implanted into subcutaneous tissue of mice. A lack of reduction in mass was demonstrated for the Vitoss BA group, as well as the absence of TRAP cells in contrast to the Vitoss scaffolds, whose mass had decreased over time.[60] In rabbits, implantation of 0.5 wt% Zn-doped magnesium phosphate bioceramics into a femoral defect showed after 90 days an increased number of osteoclasts compared to undoped bioceramics, as well as increased degradation of the material, attributing better osseointegration and bone formation to the presence of Zn.[61] The hypothesis of osteoclasts actively degrading the scaffolds is strengthened by further studies. In a sheep model with the implantation of MBGNs containing ZnO, almost no osteoclasts could be detected after 12 weeks, and at the same time, the mass of the scaffold was almost still equal to the implanted amount, indicating a lack of degradation of the material.[62] This could be explained by the anti-inflammatory properties of Zn.[14] The cell-mediated degradation of scaffolds depends largely on the inflammatory response of the introduced material. Immuno-related cell interactions also include the regulation of osteoclastogenesis.[63] In our study, a decreased activity of osteoclasts for the 3-Zn-BG group in contrast to the 0106-B1-BG group was detected. In this context, the scaffold should elicit an acceptable moderate immune response to allow the ingrowth of regeneration-relevant cells and, at the same time, have an adequate rate of degradation to allow the tissue to regenerate effectively.[63] The effect of BGs on osteoclasts seems to be of relevance and should be studied more intensively since the presence of osteoclasts and the

degradation of the material are important factors for successful bone regeneration.[64]

Bone formation *in vivo* is also largely dependent on vascular sprouting.[65,66] In the 0106-B1-BG group, CD31-positive structures were detected in the immediate surroundings of the scaffold remnants, leading to the assumption that the released ions have angiogenic potential and thus positively influence vascularization. The *in vitro* angiogenic effect of 0106-B1-BG had been reported in previous studies.[9] Meanwhile, the 3-Zn-BG showed comparable results, while the angiogenic potential of the 1393-BG remains almost the same as the empty control. Comparing these with the *in vitro* data, they are only partially in agreement. The 3-Zn-BG showed superior pro-angiogenic properties *in vitro*, especially in regard to EDN1 protein expression and in the tube formation assay using HUVECs. Growth of new blood vessels was demonstrated in femoral defects of rabbits with a Zn/Mg ion co-implanted titanium, whereas the effect was absent with co-implanted titanium alone. The combination of Zn and Mg appears to exert a beneficial influence on angiogenesis.[52] Similarly, another study showed that zinc silicate/β-tricalcium phosphate composite ceramic scaffolds containing 10 wt% Zn and Si inserted into a calvaria defect in rats increased the amount of CD31-positive cells in the newly formed tissue. The combination of Zn and Si is thought to promote the expression of CD31, thereby positively affecting vascularization.[67] MBGNs containing 5 wt% ZnO showed an increased number of blood vessels 6 weeks after implantation in a sheep model compared to their reference glass without ZnO. Interestingly, however, the expected promoting effect on bone formation did not occur, and an absence of osteoblasts and osteoclasts was demonstrated. Angiogenesis was seen here as part of the inflammatory response since the material was encapsulated *in vivo*, no diffusion, and thus no effect of the Zn ions on the surrounding tissue was possible.[62] The degradation of the material necessary for successful stimulation of bone regeneration did not take place.[68–70] There seems to be an interesting interplay *in vivo* between the anti-inflammatory property of Zn and its promoting effects on bone regeneration and angiogenesis, which should be further investigated, also in relation to the simultaneous effect of B. With respect to our study, a comparable effect on the promotion of angiogenesis could be shown *in vivo* for 0106-B1-BG and 3-Zn-BG, as well as a stronger pro-angiogenic effect of Zn-BGs *in vitro*.

5 Conclusions

The present study investigated the effects of Zn addition to the bioactive glass 0106-B1 on cytocompatibility, osteogenic, and angiogenic potential using *in vitro* and *in vivo* experimental protocols. Regarding cytocompatibility, the presence of Zn improved viability and the number of human bone marrow-derived stromal cells. A specific Zn concentration did not clearly improve the osteogenic effect in the concentration range studied. Nevertheless, the presence of Zn, regardless of its concentration, improved osteogenesis, especially at late time points. The Zn-containing BGs showed favorable angiogenic effects, which was particularly evident for EDN1 production and in the tube formation assay. The glass with the highest zinc content, 5 wt% ZnO, showed equivalent new bone formation and material degradation in the critical-size femoral defect model as the zinc-free parent glass 0106-B1. On the other hand, 0106-B1-BG showed higher osteoclast activity and vascularization in the newly formed tissue than the glass with 5 wt% ZnO. This was explained by the modulation of inflammatory processes by Zn, as described in the literature. The differences between the *in vitro* and *in vivo* performances of the BGs outline the importance of evaluating biomaterials in different experimental settings to ensure detailed characterization of the materials' biological properties, particularly in the case of BGs, characterized for their high surface bioreactivity. The supplementation of Zn into 0106-B1-BG showed promising biological potential and should, therefore, be studied more comprehensively, especially with regard to the interplay of inflammation and its impact on bone regeneration. In addition, the biological activity of 0106-B1-BG can be further modified by co-doping with other ions.

Data availability

All relevant data are included and shown within the manuscript.

Conflicts of interest

The authors declare that there are no conflicts of interest in regard to the present work.

Acknowledgements

For financial support, the authors thank the German Research Foundation (DFG), grant numbers WE6654/1-1 and BO 1191/26-1. The funding from the European Union's Horizon 2020 Research and Innovation Program, the project under grant agreement no. 739566 and financial support from the VEGA 1/0191/20 project are acknowledged. For her excellent technical support, we thank Birgit Frey. This study contains parts of the doctoral thesis of L. A. Fiehn and M. Saur.

References

1 L. L. Hench and J. R. Jones, Bioactive Glasses: Frontiers and Challenges, *Front. Bioeng. Biotechnol.*, 2015, **3**, 194.
2 F. Hohenbild, M. Arango-Ospina, A. Moghaddam, A. R. Boccaccini and F. Westhauser, Preconditioning of Bioactive Glasses before Introduction to Static Cell Culture: What Is Really Necessary?, *Methods Protoc.*, 2020, **3**(2), 38.

3 F. E. Ciraldo, E. Boccardi, V. Melli, F. Westhauser and A. R. Boccaccini, Tackling bioactive glass excessive in vitro bioreactivity: Preconditioning approaches for cell culture tests, *Acta Biomater.*, 2018, **75**, 3–10.
4 Q. Fu, M. N. Rahaman, B. S. Bal, W. Huang and D. E. Day, Preparation and bioactive characteristics of a porous 13–93 glass, and fabrication into the articulating surface of a proximal tibia, *J. Biomed. Mater. Res., Part A*, 2007, **82**(1), 222–229.
5 Q. Z. Chen, I. D. Thompson and A. R. Boccaccini, 45S5 Bioglass-derived glass-ceramic scaffolds for bone tissue engineering, *Biomaterials*, 2006, **27**(11), 2414–2425.
6 Q. Fu, M. N. Rahaman, B. S. Bal, R. F. Brown and D. E. Day, Mechanical and in vitro performance of 13–93 bioactive glass scaffolds prepared by a polymer foam replication technique, *Acta Biomater.*, 2008, **4**(6), 1854–1864.
7 M. Brink, T. Turunen, R. P. Happonen and A. Yli-Urpo, Compositional dependence of bioactivity of glasses in the system Na2O-K2O-MgO-CaO-B2O3-P2O5-SiO_2, *J. Biomed. Mater. Res.*, 1997, **37**(1), 114–121.
8 P. Balasubramanian, A. Grünewald, R. Detsch, L. Hupa, B. Jokic, F. Tallia, *et al.*, Ion Release, Hydroxyapatite Conversion, and Cytotoxicity of Boron-Containing Bioactive Glass Scaffolds, *Int. J. Appl. Glass Sci.*, 2016, **7**(2), 206–215.
9 P. Balasubramanian, L. Hupa, B. Jokic, R. Detsch, A. Grünewald and A. R. Boccaccini, Angiogenic potential of boron-containing bioactive glasses: in vitro study, *J. Mater. Sci.*, 2016, **52**(15), 8785–8792.
10 L. A. Haro Durand, G. E. Vargas, N. M. Romero, R. Vera-Mesones, J. M. Porto-Lopez, A. R. Boccaccini, *et al.*, Angiogenic effects of ionic dissolution products released from a boron-doped 45S5 bioactive glass, *J. Mater. Chem. B*, 2015, **3**(6), 1142–1148.
11 A. A. Gorustovich, J. M. Lopez, M. B. Guglielmotti and R. L. Cabrini, Biological performance of boron-modified bioactive glass particles implanted in rat tibia bone marrow, *Biomed. Mater.*, 2006, **1**(3), 100–105.
12 E. Kunisch, L. A. Fiehn, M. Saur, M. Arango-Ospina, C. Merle, S. Hagmann, *et al.*, A comparative in vitro and in vivo analysis of the biological properties of the 45S5-, 1393-, and 0106-B1-bioactive glass compositions using human bone marrow-derived stromal cells and a rodent critical size femoral defect model, *Biomater. Adv.*, 2023, **153**, 213521.
13 L. A. Fiehn, E. Kunisch, M. Saur, M. Arango-Ospina, C. Merle, S. Hagmann, *et al.*, A comparative in vitro and in vivo analysis of the impact of copper substitution on the cytocompatibility, osteogenic, and angiogenic properties of a borosilicate bioactive glass, *J. Biomed. Mater. Res., Part A*, 2024, **112**(10), 1740–1759.
14 M. Yamaguchi, Role of zinc in bone formation and bone resorption, *J. Trace Elem. Exp. Med.*, 1998, **11**(2–3), 119–135.
15 I. S. Kwun, Y. E. Cho, R. A. Lomeda, H. I. Shin, J. Y. Choi, Y. H. Kang, *et al.*, Zinc deficiency suppresses matrix mineralization and retards osteogenesis transiently with catch-up possibly through Runx 2 modulation, *Bone*, 2010, **46**(3), 732–741.
16 F. Westhauser, S. Decker, Q. Nawaz, F. Rehder, S. Wilkesmann, A. Moghaddam, *et al.*, Impact of Zinc- or Copper-Doped Mesoporous Bioactive Glass Nanoparticles on the Osteogenic Differentiation and Matrix Formation of Mesenchymal Stromal Cells, *Materials*, 2021, **14**(8), 1864.
17 A. Ali, A. Paladhi, S. K. Hira, B. N. Singh and R. Pyare, Bioactive ZnO-assisted 1393 glass scaffold promotes osteogenic differentiation: Some studies, *J. Biomed. Mater. Res., Part B*, 2022, 1059–1073.
18 B. Widholz, S. Tsitlakidis, B. Reible, A. Moghaddam and F. Westhauser, Pooling of Patient-Derived Mesenchymal Stromal Cells Reduces Inter-Individual Confounder-Associated Variation without Negative Impact on Cell Viability, Proliferation and Osteogenic Differentiation, *Cells*, 2019, **8**(6), 633.
19 E. Kunisch, S. Maenz, M. Knoblich, F. Ploeger, K. D. Jandt, J. Bossert, *et al.*, Short-time pre-washing of brushite-forming calcium phosphate cement improves its in vitro cytocompatibility, *Tissue Cell*, 2017, **49**(6), 697–710.
20 G. Carpentier, S. Berndt, S. Ferratge, W. Rasband, M. Cuendet, G. Uzan, *et al.*, Angiogenesis Analyzer for ImageJ - A comparative morphometric analysis of "Endothelial Tube Formation Assay" and "Fibrin Bead Assay", *Sci. Rep.*, 2020, **10**(1), 11568.
21 T. A. Freeman, P. Patel, J. Parvizi, V. Antoci Jr and I. M. Shapiro, Micro-CT analysis with multiple thresholds allows detection of bone formation and resorption during ultrasound-treated fracture healing, *J. Orthop. Res.*, 2009, **27**(5), 673–679.
22 J. Brocher, P. Janicki, P. Voltz, E. Seebach, E. Neumann, U. Mueller-Ladner, *et al.*, Inferior ectopic bone formation of mesenchymal stromal cells from adipose tissue compared to bone marrow: rescue by chondrogenic pre-induction, *Stem Cell Res.*, 2013, **11**(3), 1393–1406.
23 M. Hoellig, F. Westhauser, K. Kornienko, K. Xiao, G. Schmidmaier and A. Moghaddam, Mesenchymal stem cells from reaming material possess high osteogenic potential and react sensitively to bone morphogenetic protein 7, *J. Appl. Biomater. Funct. Mater.*, 2017, **15**(1), e54–e62.
24 F. Westhauser, A. S. Senger, D. Obert, F. E. Ciraldo, K. Schuhladen, G. Schmidmaier, *et al.*, Gelatin coating increases in vivo bone formation capacity of three-dimensional 45S5 bioactive glass-based crystalline scaffolds, *J. Tissue Eng. Regener. Med.*, 2019, **13**(2), 179–190.
25 F. Westhauser, M. Karadjian, C. Essers, A. S. Senger, S. Hagmann, G. Schmidmaier, *et al.*, Osteogenic differentiation of mesenchymal stem cells is enhanced in a 45S5-supplemented beta-TCP composite scaffold: an *in vitro* comparison of Vitoss and Vitoss BA, *PLoS One*, 2019, **14**(2), e0212799.
26 J. E. Gough, J. R. Jones and L. L. Hench, Nodule formation and mineralisation of human primary osteoblasts cultured on a porous bioactive glass scaffold, *Biomaterials*, 2004, **25**(11), 2039–2046.
27 H. Z. Movat, Demonstration of all connective tissue elements in a single section; pentachrome stains, *AMA Arch. Pathol.*, 1955, **60**(3), 289–295.

28 F. Westhauser, B. Widholz, Q. Nawaz, S. Tsitlakidis, S. Hagmann, A. Moghaddam, *et al.*, Favorable angiogenic properties of the borosilicate bioactive glass 0106-B1 result in enhanced in vivo osteoid formation compared to 45S5 Bioglass, *Biomater. Sci.*, 2019, **7**(12), 5161–5176.
29 S. Minkwitz, M. Fassbender, Z. Kronbach and B. Wildemann, Longitudinal analysis of osteogenic and angiogenic signaling factors in healing models mimicking atrophic and hypertrophic non-unions in rats, *PLoS One*, 2015, **10**(4), e0124217.
30 M. Widbiller, C. Rothmaier, D. Saliter, M. Wolflick, A. Rosendahl, W. Buchalla, *et al.*, Histology of human teeth: Standard and specific staining methods revisited, *Arch. Oral Biol.*, 2021, **127**, 105136.
31 A. R. Hayman, Tartrate-resistant acid phosphatase (TRAP) and the osteoclast/immune cell dichotomy, *Autoimmunity*, 2008, **41**(3), 218–223.
32 R. A. Armstrong, When to use the Bonferroni correction, *Ophthalmic Physiol. Opt.*, 2014, **34**(5), 502–508.
33 A. Hoppe, N. S. Guldal and A. R. Boccaccini, A review of the biological response to ionic dissolution products from bioactive glasses and glass-ceramics, *Biomaterials*, 2011, **32**(11), 2757–2774.
34 M. Y. Shie, S. J. Ding and H. C. Chang, The role of silicon in osteoblast-like cell proliferation and apoptosis, *Acta Biomater.*, 2011, **7**(6), 2604–2614.
35 V. Aina, A. Perardi, L. Bergandi, G. Malavasi, L. Menabue, C. Morterra, *et al.*, Cytotoxicity of zinc-containing bioactive glasses in contact with human osteoblasts, *Chem.-Biol. Interact.*, 2007, **167**(3), 207–218.
36 H. Wang, S. Zhao, W. Xiao, X. Cui, W. Huang, M. N. Rahaman, *et al.*, Three-dimensional zinc incorporated borosilicate bioactive glass scaffolds for rodent critical-sized calvarial defects repair and regeneration, *Colloids Surf., B*, 2015, **130**, 149–156.
37 J. Bejarano, P. Caviedes and H. Palza, Sol-gel synthesis and in vitro bioactivity of copper and zinc-doped silicate bioactive glasses and glass-ceramics, *Biomed. Mater.*, 2015, **10**(2), 025001.
38 I. Sahibdad, S. Khalid, G. R. Chaudhry, A. Salim, S. Begum and I. Khan, Zinc enhances the cell adhesion, migration, and self-renewal potential of human umbilical cord derived mesenchymal stem cells, *World J. Stem Cells*, 2023, **15**(7), 751–767.
39 P. Balasubramanian, L. A. Strobel, U. Kneser and A. R. Boccaccini, Zinc-containing bioactive glasses for bone regeneration, dental and orthopedic applications, *Biomed. Glasses*, 2015, **1**(1), 51–69.
40 M. Molenda and J. Kolmas, The Role of Zinc in Bone Tissue Health and Regeneration-a Review, *Biol. Trace Elem. Res.*, 2023, 5640–5651.
41 M. Yamaguchi and R. Yamaguchi, Action of zinc on bone metabolism in rats. Increases in alkaline phosphatase activity and DNA content, *Biochem. Pharmacol.*, 1986, **35**(5), 773–777.
42 I. Nikolic-Hughes, P. J. O'Brien and D. Herschlag, Alkaline phosphatase catalysis is ultrasensitive to charge sequestered between the active site zinc ions, *J. Am. Chem. Soc.*, 2005, **127**(26), 9314–9315.
43 A. Igarashi and M. Yamaguchi, Great increase in bone 66 kDa protein and osteocalcin at later stages with healing rat fractures: effect of zinc treatment, *Int. J. Mol. Med.*, 2003, **11**(2), 223–228.
44 K. Yusa, O. Yamamoto, M. Fukuda, S. Koyota, Y. Koizumi and T. Sugiyama, In vitro prominent bone regeneration by release zinc ion from Zn-modified implant, *Biochem. Biophys. Res. Commun.*, 2011, **412**(2), 273–278.
45 X. Ying, S. Cheng, W. Wang, Z. Lin, Q. Chen, W. Zhang, *et al.*, Effect of boron on osteogenic differentiation of human bone marrow stromal cells, *Biol. Trace Elem. Res.*, 2011, **144**(1–3), 306–315.
46 S. Decker, M. Arango-Ospina, F. Rehder, A. Moghaddam, R. Simon, C. Merle, *et al.*, In vitro and in ovo impact of the ionic dissolution products of boron-doped bioactive silicate glasses on cell viability, osteogenesis and angiogenesis, *Sci. Rep.*, 2022, **12**(1), 8510.
47 C. Wu, R. Miron, A. Sculean, S. Kaskel, T. Doert, R. Schulze, *et al.*, Proliferation, differentiation and gene expression of osteoblasts in boron-containing associated with dexamethasone deliver from mesoporous bioactive glass scaffolds, *Biomaterials*, 2011, **32**(29), 7068–7078.
48 E. Birmingham, G. L. Niebur, P. E. McHugh, G. Shaw, F. P. Barry and L. M. McNamara, Osteogenic differentiation of mesenchymal stem cells is regulated by osteocyte and osteoblast cells in a simplified bone niche, *Eur. Cells Mater.*, 2012, **23**, 13–27.
49 M. F. Pittenger, A. M. Mackay, S. C. Beck, R. K. Jaiswal, R. Douglas, J. D. Mosca, *et al.*, Multilineage potential of adult human mesenchymal stem cells, *Science*, 1999, **284**(5411), 143–147.
50 V. Aina, G. Malavasi, A. Fiorio Pla, L. Munaron and C. Morterra, Zinc-containing bioactive glasses: surface reactivity and behaviour towards endothelial cells, *Acta Biomater.*, 2009, **5**(4), 1211–1222.
51 D. Zhang, Y. Li, T. Zhu, F. Zhang, Z. Yang and D. Miao, Zinc supplementation results in improved therapeutic potential of bone marrow-derived mesenchymal stromal cells in a mouse ischemic limb model, *Cytotherapy*, 2011, **13**(2), 156–164.
52 Y. Yu, G. Jin, Y. Xue, D. Wang, X. Liu and J. Sun, Multifunctions of dual Zn/Mg ion co-implanted titanium on osteogenesis, angiogenesis and bacteria inhibition for dental implants, *Acta Biomater.*, 2017, **49**, 590–603.
53 D. Salani, G. Taraboletti, L. Rosano, V. Di Castro, P. Borsotti, R. Giavazzi, *et al.*, Endothelin-1 induces an angiogenic phenotype in cultured endothelial cells and stimulates neovascularization in vivo, *Am. J. Pathol.*, 2000, **157**(5), 1703–1711.
54 R. Augustine, P. Dan, A. Sosnik, N. Kalarikkal, N. Tran, B. Vincent, *et al.*, Electrospun poly(vinylidene fluoride-trifluoroethylene)/zinc oxide nanocomposite tissue engineering scaffolds with enhanced cell adhesion and blood vessel formation, *Nano Res.*, 2017, **10**(10), 3358–3376.

55 J. Ma, N. Zhao and D. Zhu, Endothelial Cellular Responses to Biodegradable Metal Zinc, *ACS Biomater. Sci. Eng.*, 2015, **1**(11), 1174–1182.
56 E. J. Mackie, Y. A. Ahmed, L. Tatarczuch, K. S. Chen and M. Mirams, Endochondral ossification: how cartilage is converted into bone in the developing skeleton, *Int. J. Biochem. Cell Biol.*, 2008, **40**(1), 46–62.
57 G. Lusvardi, D. Zaffe, L. Menabue, C. Bertoldi, G. Malavasi and U. Consolo, In vitro and in vivo behaviour of zinc-doped phosphosilicate glasses, *Acta Biomater.*, 2009, **5**(1), 419–428.
58 C. S. Bahney, R. L. Zondervan, P. Allison, A. Theologis, J. W. Ashley, J. Ahn, *et al.*, Cellular biology of fracture healing, *J. Orthop. Res.*, 2019, **37**(1), 35–50.
59 R. L. Bighetti-Trevisan, A. T. P. Souza, I. W. Tosin, N. P. Bueno, M. C. Crovace, M. M. Beloti, *et al.*, Bioactive glass-ceramic for bone tissue engineering: an in vitro and in vivo study focusing on osteoclasts, *Braz. Oral Res.*, 2022, **36**, e022.
60 F. Westhauser, C. Essers, M. Karadjian, B. Reible, G. Schmidmaier, S. Hagmann, *et al.*, Supplementation with 45S5 Bioactive Glass Reduces In Vivo Resorption of the beta-Tricalcium-Phosphate-Based Bone Substitute Material Vitoss, *Int. J. Mol. Sci.*, 2019, **20**(17), 4253.
61 K. Sarkar, V. Kumar, K. B. Devi, D. Ghosh, S. K. Nandi and M. Roy, Anomalous in Vitro and in Vivo Degradation of Magnesium Phosphate Bioceramics: Role of Zinc Addition, *ACS Biomater. Sci. Eng.*, 2019, **5**(10), 5097–5106.
62 J. Jimenez-Holguin, D. Arcos, D. Lozano, M. Saiz-Pardo, D. de Pablo, L. Ortega, *et al.*, In Vitro and In Vivo Response of Zinc-Containing Mesoporous Bioactive Glasses in a Sheep Animal Model, *Int. J. Mol. Sci.*, 2022, **23**(22), 13918.
63 D. Yang, J. Xiao, B. Wang, L. Li, X. Kong and J. Liao, The immune reaction and degradation fate of scaffold in cartilage/bone tissue engineering, *Mater. Sci. Eng., C*, 2019, **104**, 109927.
64 R. Detsch and A. R. Boccaccini, The role of osteoclasts in bone tissue engineering, *J. Tissue Eng. Regener. Med.*, 2015, **9**(10), 1133–1149.
65 S. M. Chim, J. Tickner, S. T. Chow, V. Kuek, B. Guo, G. Zhang, *et al.*, Angiogenic factors in bone local environment, *Cytokine Growth Factor Rev.*, 2013, **24**(3), 297–310.
66 U. Saran, S. Gemini Piperni and S. Chatterjee, Role of angiogenesis in bone repair, *Arch. Biochem. Biophys.*, 2014, **561**, 109–117.
67 X. Yuan, T. Lu, F. He, T. Wu, X. Wang and J. Ye, 3D-plotted zinc silicate/beta-tricalcium phosphate ceramic scaffolds enable fast osteogenesis by activating the p38 signaling pathway, *J. Mater. Chem. B*, 2022, **10**(46), 9639–9653.
68 A. R. Amini, C. T. Laurencin and S. P. Nukavarapu, Bone tissue engineering: recent advances and challenges, *Crit. Rev. Biomed. Eng.*, 2012, **40**(5), 363–408.
69 D. W. Hutmacher, J. T. Schantz, C. X. Lam, K. C. Tan and T. C. Lim, State of the art and future directions of scaffold-based bone engineering from a biomaterials perspective, *J. Tissue Eng. Regener. Med.*, 2007, **1**(4), 245–260.
70 R. J. O'Keefe and J. Mao, Bone tissue engineering and regeneration: from discovery to the clinic–an overview, *Tissue Eng., Part B*, 2011, **17**(6), 389–392.